A Model for the Earthquake Cycle in Underthrust Zones

WAYNE THATCHER

U.S. Geological Survey, Menlo Park, California 94025

JOHN B. RUNDLE

Sandia Laboratories, Albuquerque, New Mexico 87115

The time-dependent surface deformation due to thrust faulting in an elastic plate overlying a viscoelastic half space is examined and compared with geodetic measurements of earthquake-related crustal movements from Japan. The model fault is two-dimensional, and the half-space rheology is that of a Maxwell solid whose instantaneous response to applied loads is purely elastic but which subsequently flows to relieve imposed shear stresses. A characteristic feature of shallow-angle underthrusting shown by these computations is that buried slip produces predominantly land uplift, while asthenospheric relaxation due to surface faulting results principally in surface downwarping. These distinctive patterns, also reflected in the measured deformation, are particularly useful in formulating a viable model for the entire earthquake cycle. For the model constructed in this way, coseismic faulting in the upper part of the plate transfers a load to the lower lithosphere and asthenosphere, inducing postseismic slip downdip of the seismic rupture and relaxation in the asthenosphere, these transients eventually merging into the steady buried slip and smoother asthenospheric flow that characterize the interseismic phase of the deformation cycle. Aseismic slip and asthenospheric relaxation cause the load supported by the plate-bounding fault to be gradually transferred back to the shallow locked segment of the fault, effecting the strain buildup for a subsequent earthquake, and the cycle is repeated. No explicit account of plate-driving forces is made; their net effect is presumed to be the steady buried slip that persists throughout the cycle and provides the energy that drives it. Characteristic features of the observed deformation in southwest Japan, site of the 1946 Nankaido earthquake, and in the South Kanto district, where the great 1923 earthquake occurred, are matched by this model using conventional values of lithospheric thickness (60 km) and asthenospheric viscosity (10^{21} P, or 10^{20} N s/m^2), although the model is not strongly tied to these exact values. Postseismic movements are adequately explained by episodic slip that occurs below the coseismic rupture, is 10–30% of the seismic slip, and acts in the same sense. Superimposed on these movements are the lesser effects of asthenospheric relaxation, which in the South Kanto district contribute significantly to the postseismic vertical level changes because post-1923 buried slip is comparatively small and involves largely strike slip movements. Interseismic subsidence in both regions is explained well by asthenospheric relaxation and less significant deformation effects due to steady aseismic slip on the lower part of the plate boundary.

1. INTRODUCTION

The plate tectonic view that the earth's surface is a mosaic of strong elastic plates that overlie a relatively weaker viscous asthenosphere provides a conceptual framework that successfully accounts for a diverse assemblage of geologic and geophysical observations. Several important implications of this model for the crustal deformation occurring at plate boundaries are now being recognized, and a number of recent studies have suggested that the geodetically measured deformation observed in active seismic zones may be due to time-dependent flow in the asthenosphere induced by the sudden stress drop resulting from major earthquakes in the overlying lithosphere [*Nur and Mavko,* 1974; *Smith,* 1974; *Rundle and Jackson,* 1977; *Spence and Turcotte,* 1978; *Savage and Prescott,* 1978*b*]. On the other hand, it is not clear to what extent it is necessary to account for the nonelastic response of the asthenosphere in order to explain observed plate boundary deformation. The purely coseismic deformation from large earthquakes is now well understood, and numerous studies have shown that observed movements are adequately explained by slippage on faults modeled using elastic dislocation theory [e.g., *Chinnery,* 1961; *Hastie and Savage,* 1970, *Ando,* 1971]. Furthermore, many features of geodetically measured aseismic movements can be adequately explained by purely elastic models in which both the time-dependent postseismic deformation and the relatively steady interseismic secular movements are attributed to episodic or steady aseismic slip on the downward extension of the fault plane that ruptured coseismically [*Savage and Burford,* 1970, 1973; *Thatcher,* 1974, 1975; *Shimazaki,* 1974; *Kasahara,* 1975; *Brown et al.,* 1977; *Scholz and Kato,* 1978]. However, these models are certainly nonunique, and at present there is no clear consensus on whether or not the flow properties of the asthenosphere directly affect geodetically measured deformation at plate boundaries.

This lack of uniqueness is underlined by recent work [*Rundle and Jackson,* 1977; *Spence and Turcotte,* 1979; *Savage and Prescott,* 1978*b*] which demonstrates that for a strike slip transform fault in the lithosphere the effects of buried slip and asthenospheric relaxation are very similar, satisfy available data about equally well, and may be observationally indistinguishable. Choosing between these alternatives then depends on assumed choices for lithospheric thickness and asthenospheric viscosity, and the permissible range of these rather poorly constrained parameters seems wide enough to admit either viewpoint.

For several reasons we believe the situation is more promising for the case of reverse dip slip faulting at subduction zones. Our results show that in contrast with the strike slip problem, for dip slip faulting the deformation due to buried slip differs characteristically from that due to the asthenospheric relaxation that follows surface faulting (Figure 1). Furthermore, observations of the spatial distribution and time-dependent behavior of postseismic and interseismic movements associated with thrust faulting are relatively more complete than corresponding measurements from strike slip plate bounda-

Paper number 9B0668.

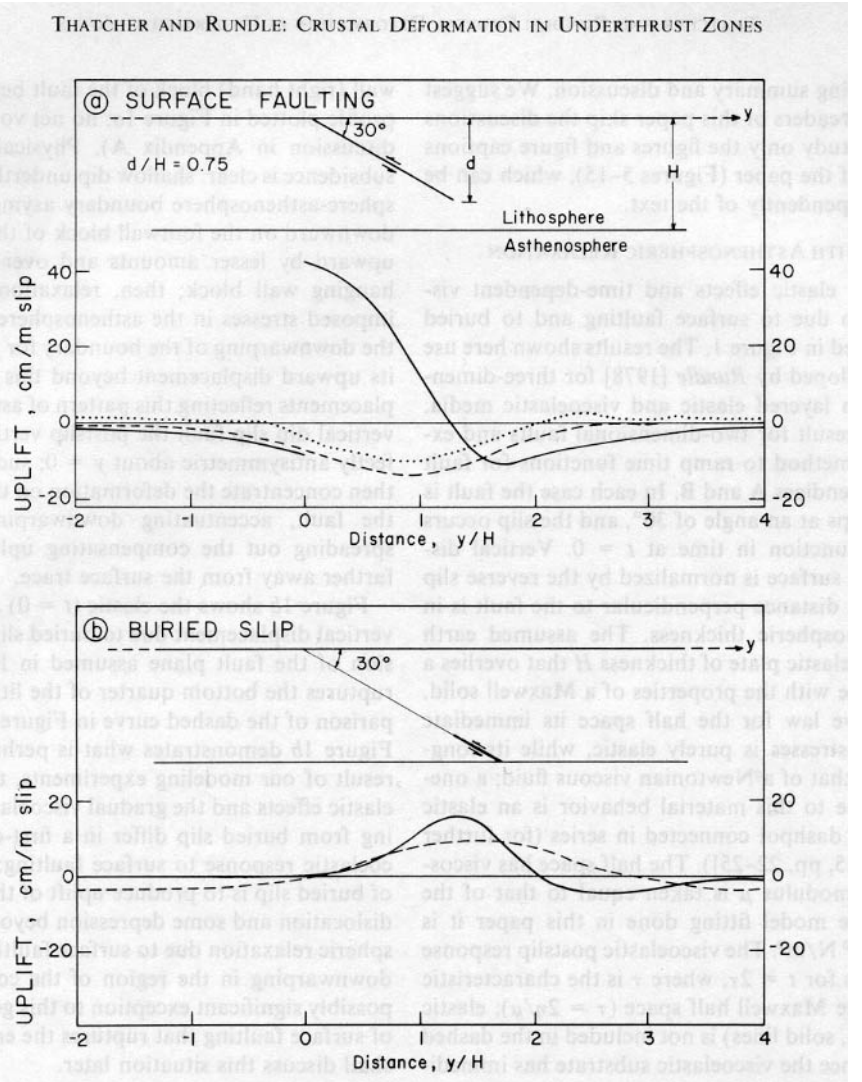

Fig. 1. (*a*) Coseismic vertical displacement ($t = 0$, solid line) and subsequent viscoelastic response ($t = 2\tau$; dotted line, compressibility of half space held constant; dashed line, λ fixed) due to slip on a fault rupturing three quarters of an elastic plate of thickness H overlying a viscoelastic (Maxwell) half space. Vertical uplift is normalized by the reverse fault slip, and distance perpendicular to the fault, y, is in multiples of the lithospheric thickness H. Fault dip is 30°. (*b*) Similar to Figure 1*a* but for buried slip extending from a depth of three quarters of the lithospheric thickness to its base.

ries. These observations, principally from Japan, place further constraints on modeling, and comparisons between computed and observed deformation suggest that characteristic features of asthenospheric relaxation and buried slip can be clearly distinguished in the observations. Briefly put, these comparisons suggest that movements observed landward of subduction zones may be understood as being due primarily to a superposition of two effects; the partioning differs somewhat from region to region but is characterized dominantly by episodic buried slip in the postseismic interval and by subsidence due to asthenospheric relaxation during the interseismic phase of the deformation.

Previous studies have taken rather different viewpoints. Several investigators have shown that postseismic movements could be explained by episodic buried slip that acts in the same sense as the shallower coseismic slippage [*Thatcher,* 1974, 1975; *Kasahara,* 1975; *Brown et al.,* 1977]. Others have suggested that to explain some measurements in underthrust zones requires postseismic slip that acts in a sense opposite to the coseismic fault slip [*Fitch and Scholz,* 1971; *Scholz and Kato,* 1978]. While the present study has attributed most of the interseismic secular deformation at subduction zones to the effects of asthenospheric relaxation, earlier work [*Nur and Mavko,* 1974; *Smith,* 1974; *Rundle and Jackson,* 1977] has focused on explaining postseismic movements with this mechanism.

The downward pull of the underthrust lithospheric plate provides an intuitively appealing explanation for the interseismic subsidence observed landward of trenches [*Mogi,* 1970; *Fitch and Scholz,* 1971; *Shimazaki,* 1974]. While our interpretation differs somewhat from this view, its underlying philosophy is the same: plate-driving forces are ultimately responsible, since in the model we are proposing it is these forces that supply the energy for strain buildup, leading to the abrupt failure of the plate boundary that induces asthenospheric readjustments.

This paper is organized into eight sections. Following the introduction, section 2 considers the time-dependent surface deformation for a faulting model in which the effects of a viscoelastic asthenosphere are included. In section 3 these results are used to construct a model for the complete deformation cycle. The relation of this model to the broader-scale processes of plate tectonics is discussed, and some of the idealizations implicit in our approach are mentioned. Sections 4–7 justify the model by comparing its predictions with extensive observations from central and southwest Japan. Finally,

section 8 is a concluding summary and discussion. We suggest that the more casual readers of this paper skip the discussions of sections 4–7 and study only the figures and figure captions related to that part of the paper (Figures 5–15), which can be followed largely independently of the text.

2. Models With Asthenospheric Relaxation

The instantaneous elastic effects and time-dependent viscoelastic deformation due to surface faulting and to buried fault slip are compared in Figure 1. The results shown here use the formulation developed by *Rundle* [1978] for three-dimensional dislocations in layered elastic and viscoelastic media. Simplifications that result for two-dimensional faults and extension of Rundle's method to ramp time functions for fault slip are given in Appendices A and B. In each case the fault is infinitely long and dips at an angle of 30°, and the slip occurs abruptly as a step function in time at $t = 0$. Vertical displacement at the free surface is normalized by the reverse slip on the fault, and the distance perpendicular to the fault is in multiples of the lithospheric thickness. The assumed earth model consists of an elastic plate of thickness H that overlies a viscoelastic half space with the properties of a Maxwell solid. With this constitutive law for the half space its immediate response to applied stresses is purely elastic, while its long-term deformation is that of a Newtonian viscous fluid; a one-dimensional analogue to this material behavior is an elastic spring and a viscous dashpot connected in series (for further details, see *Fung* [1965, pp. 22–25]). The half space has viscosity η, and its shear modulus μ is taken equal to that of the elastic plate. For the model fitting done in this paper it is assumed $\mu = 6 \times 10^{10}$ N/m^2. The viscoelastic postslip response plotted in Figure 1 is for $t = 2\tau$, where τ is the characteristic relaxation time of the Maxwell half space ($\tau = 2\eta/\mu$); elastic uplift ($t = 0$ response, solid lines) is not included in the dashed curves for $t = 2\tau$. Since the viscoelastic substrate has immediate elastic properties that are identical to those of the overlying plate, the $t = 0$ deformation should be the same as that for faulting in an elastic half space; that this in fact is the case is one check on the correctness of our calculations.

For surface faulting (Figure 1*a*), two cases of viscoelastic postslip response are plotted. In both, the shear modulus μ of the half space is taken to be Maxwell viscoelastic. The dashed curve shows the results when the Lamé constant λ for the half space is held constant, and the dotted curve illustrates the surface deformation that results when the compressibility K is fixed. The profiles are very similar, and it seems unlikely that the slightly different rheological assumptions can be distinguished on the basis of plate boundary observations. Both assumptions have been used in modeling the surface uplift in Fennoscandia and arctic Canada that followed the melting of continental ice sheets in these regions [*Walcott*, 1973; *Peltier*, 1976]. Opinions differ on which rheology to assume, but the differences are not critical in the modeling carried out in this paper. In what follows we will take λ constant and μ Maxwell viscoelastic, implying a small viscoelastic relaxation of the bulk modulus K.

Figure 1*a* shows the coseismic and subsequent viscoelastic deformation for a fault that ruptures the free surface and extends through three quarters of the lithosphere ($d/H = 0.75$). The most important feature illustrated by the viscoelastic deformation profile (dashed curve) is that the effect of the asthenosphere is to produce postslip downwarping over a broad region near the fault, even in parts of the profile that subsided coseismically (minor amounts of uplift occur on the hanging wall (right hand) block of the fault beyond the segment of the profile plotted in Figure 1*a*; no net volume changes occur; see discussion in Appendix A). Physically, the reason for this subsidence is clear: shallow dip underthrusting warps the lithosphere-asthenosphere boundary asymmetrically, deforming it downward on the footwall block of the fault and displacing it upward by lesser amounts and over a wider region on the hanging wall block; then, relaxation of these coseismically imposed stresses in the asthenosphere progressively increases the downwarping of the boundary for $y/H \lesssim 1.5$ and enhances its upward displacement beyond this point, with surface displacements reflecting this pattern of asthenospheric flow. For a vertical dip slip fault the postslip vertical displacement is perfectly antisymmetric about $y = 0$; successively shallower dips then concentrate the deformation on the hanging wall block of the fault, accentuating downwarping near the fault and spreading out the compensating uplift over a wider region farther away from the surface trace.

Figure 1*b* shows the elastic ($t = 0$) and viscoelastic ($t = 2\tau$) vertical displacement due to buried slip on the downdip extension of the fault plane assumed in Figure 1*a*. This slippage ruptures the bottom quarter of the lithospheric plate. A comparison of the dashed curve in Figure 1*a* with both profiles in Figure 1*b* demonstrates what is perhaps the most significant result of our modeling experiments, that both the immediate elastic effects and the gradual viscoelastic deformations resulting from buried slip differ in a first-order way from the viscoelastic response to surface faulting: the predominant effect of buried slip is to produce uplift of the free surface above the dislocation and some depression beyond it, while the asthenospheric relaxation due to surface faulting results in widespread downwarping in the region of the coseismic deformation. A possibly significant exception to this general rule is for the case of surface faulting that ruptures the entire lithosphere, and we shall discuss this situation later.

Now, however, we return to the surface faulting model of Figure 1*a* and examine the spatial pattern and time dependence of the viscoelastic surface deformation in more detail. Figure 2*a* is a plot of the cumulative postslip viscoelastic displacements for successive times from 0.1τ to 2.0τ. The figure shows that although the cumulative displacements increase monotonically with time, the general shape of the profile remains unchanged, i.e., there is little evidence for any lateral migration of the deformation with time away from the region of sudden fault slip at $t = 0$. As *Savage and Prescott* [1978*a*] have pointed out, the absence of such a strain migration effect is due to the instantaneous elasticity of the Maxwell half space: stresses imposed on the asthenosphere coseismically relax viscoelastically after $t = 0$, whereas with a purely viscous rheology, only the plate responds elastically, and the subsequent adjustment of the asthenosphere produces the wavelike migration effects discussed by *Elsasser* [1969], *Bott and Dean* [1973], *Anderson* [1975], and *Melosh* [1976]. Since, for example, the earth's mantle efficiently transmits transverse seismic waves, we agree with *Savage and Prescott* [1978*a*] that for modeling earthquake-induced effects in the asthenosphere a Maxwell rheology is more nearly correct than is a purely viscous constitutive law. However, as *Melosh* [1978] has emphasized, some forms of nonlinear asthenospheric rheology do predict deformation migration effects that are absent from the linear case.

The time dependence of vertical movements at selected surface locations is shown in Figure 2*b*. The most striking feature of these curves is that in the region of large postslip deforma-

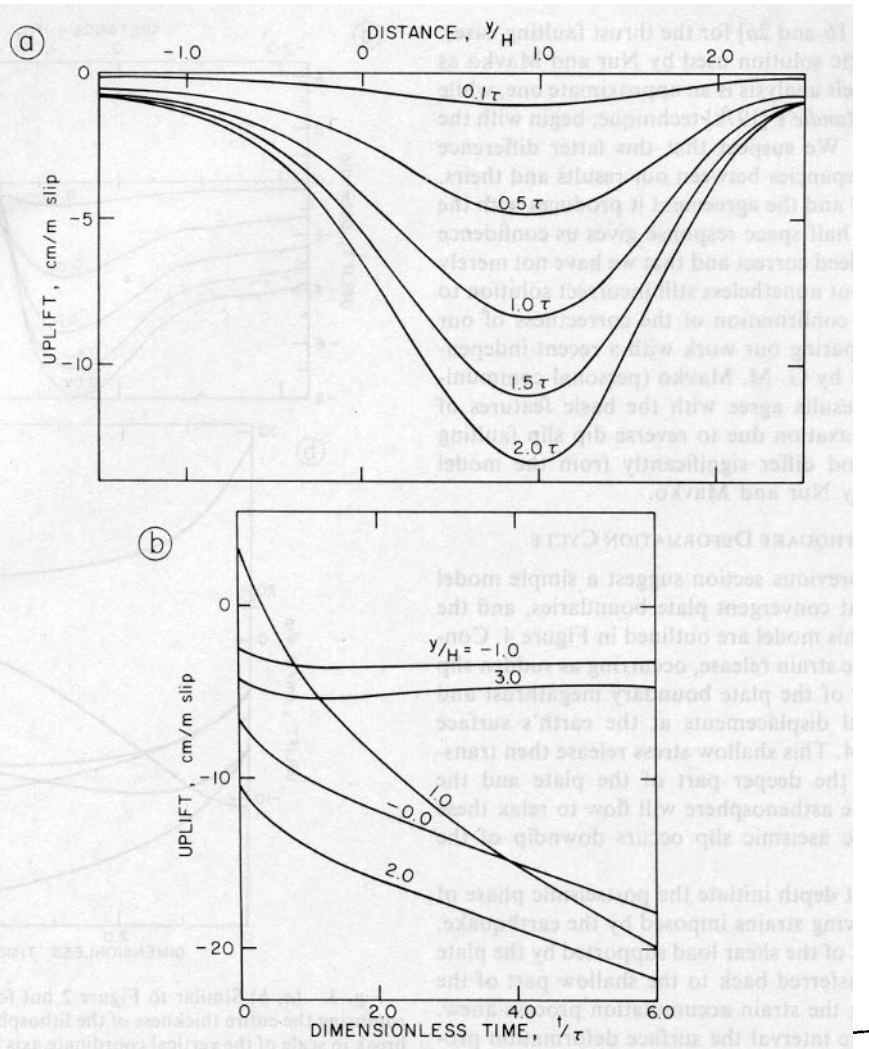

Fig. 2. (*a*) Cumulative viscoelastic (postslip) vertical displacement versus distance for successively longer times following sudden slip on a thrust fault that ruptures three quarters of the lithospheric thickness (model of Figure 1*a*, top). Distance perpendicular to the fault, y, is normalized by the lithospheric thickness H, and vertical uplift is in centimeters per meter of fault slip. Time units are in terms of the asthenospheric relaxation time τ. (Note that if the half-space viscosity is about 10^{21} P, or 10^{20} N/m^2, then $\tau \simeq 100$ years.) (*b*) Vertical displacement history at selected values of y/H for the same model as in Figure 2*a*. Offset at $t/\tau = 0$ is the coseismic displacement at each point.

tion (roughly from $y/H = -0.5$ to $+2.0$), movements persist for many asthenospheric relaxation times and do not, for example, simply decay exponentially with characteristic time τ. This feature is a general property of plate-asthenosphere models, and similar time-dependent movements of long duration are shown for the corresponding strike slip problem [*Spence and Turcotte,* 1979] and in models of glacioisostatic uplift [*Walcott,* 1973]. Note also from Figure 2*b* that the surface displacements show a time dependence that varies with position, so that if each curve were fit empirically to an exponential decay, inferred decay times would not only fail to reflect the true relaxation time of the asthenosphere but would also vary significantly with position.

Figure 3 is similar to Figure 2 but shows the space and time dependence of the viscoelastic deformation that results from rupture of the entire lithosphere. The plate-wide thrust fault dips 30°, and hence this model is simply a superposition of the models of Figures 1*a* and 1*b*. Comparison of Figure 3 with Figures 1*a* and 2 reveals some significant differences, the most striking of which is that for the plate-wide rupture there is substantial postslip uplift centered near $y/H = 2$ (Figure 3*a*), which continues to grow steadily for long times after $t = 0$ ($y/H = 2.0$ curve, Figure 3*b*). In addition, the postslip deformation extends somewhat farther into the plate, and the time dependence (Figure 3*b*) is more diverse and shows greater spatial variation than does the model in which only part of the plate is faulted coseismically.

The results shown in Figure 1*a*, both for the coseismic and postslip deformation, differ substantially from those obtained previously by *Nur and Mavko* [1974]. The model parameters used in Figure 1*a* are identical to those chosen by them with the exception of the assumed asthenospheric rheology, which we have taken to be the constitutive law for a Maxwell solid but which Nur and Mavko assume to be a standard linear solid. However, this single difference cannot explain the discrepancies, since computations we have carried out for a standard linear solid asthenosphere are similar to the results shown in Figure 1*a* but remain quite different from Nur and Mavko's results. Two lines of evidence support the correctness of our calculations. First, our coseismic uplift profile agrees, as it should, with that computed for faulting in an elastic half space, while Nur and Mavko's does not (refer to *Nur and*

Mavko [1974, Figures 1*b* and 2*a*] for the thrust faulting case). Furthermore, the elastic solution used by Nur and Mavko as the starting point in their analysis is an approximate one, while our results, applying *Rundle*'s [1978] technique, begin with the exact elastic solution. We suspect that this latter difference accounts for the discrepancies between our results and theirs. Our exact formulation and the agreement it produces with the expected $t = 0$ elastic half space response gives us confidence that our results are indeed correct and that we have not merely generated a different but nonetheless still incorrect solution to the problem. Further confirmation of the correctness of our results comes by comparing our work with a recent independent calculation made by G. M. Mavko (personal communication, 1978); these results agree with the basic features of the asthenospheric relaxation due to reverse dip slip faulting that we show here and differ significantly from the model originally presented by Nur and Mavko.

3. The Earthquake Deformation Cycle

The results of the previous section suggest a simple model for the seismic cycle at convergent plate boundaries, and the principal features of this model are outlined in Figure 4. Consider first the coseismic strain release, occurring as sudden slip on the shallower part of the plate boundary megathrust and producing the vertical displacements at the earth's surface labeled CO in Figure 4. This shallow stress release then transfers a shear load to the deeper part of the plate and the asthenosphere, and the asthenosphere will flow to relax these stresses while episodic aseismic slip occurs downdip of the coseismic fault plane.

These movements at depth initiate the postseismic phase of the deformation, relieving strains imposed by the earthquake. At the same time, part of the shear load supported by the plate boundary fault is transferred back to the shallow part of the lithosphere, beginning the strain accumulation process anew. During the postseismic interval the surface deformation profile will be some combination of asthenospheric relaxation due to surface faulting (dashed curve, Figure 1*a*) and the elastic and viscoelastic responses to buried slip (solid and dashed curves, Figure 1*b*), the exact proportions of each depending on the d/H ratio, the amount of coseismic slip, the asthenospheric relaxation time, and the amount and extent of episodic postearthquake slip. If episodic slip is the dominant process, the resulting uplift profile will be similar to the dashed curve labeled POST in Figure 4.

Once the more rapid effects of asthenospheric adjustment and episodic slip have died away, the postseismic movements should merge into the pattern of interseismic secular deformation. Surface straining occurs at an approximately uniform rate that reflects both the nearly constant rate of asthenospheric relaxation and the more or less steady deep aseismic slip that is driven by the convergence of the plates. Once again, the surface displacements during this phase of the movement cycle will be a superposition of the dashed profile of Figure 1*a* and the two curves plotted in Figure 1*b* (INTER curve, Figure 4). Both processes increase shear stresses in the shallow lithosphere near the plate boundary, and once the static strength of the brittle coseismic fault segment is exceeded, a great earthquake occurs, and the cycle begins once more.

Relation to Tectonic Plate Movements

It is worthwhile emphasizing that the model proposed here is a kinematic one that takes no explicit account of the forces that drive the plates and ultimately supply the strain energy to maintain the earthquake cycle. Whatever these forces may be, in our model their net effect on plate boundary deformation is due *solely* to the steady aseismic buried slip that persists throughout the cycle. The plate movement is reflected in this steady slip, and its rate is determined by the relative plate motion rate. The buried slip continually loads the shallow locked seismic zone, and it is in this way that the plate motion rate is related to the strain accumulation rate and hence the recurrence interval. In addition, postearthquake flow in the asthenosphere contributes to the reloading, transferring stresses that were imposed coseismically back into the overlying lithosphere at a rate that depends on the asthenospheric viscosity. Thus in our model the plate boundary processes are understood as an essentially local interaction between seismic and aseismic slip on the megathrust and the viscoelastic relaxation of the asthenosphere to these loads.

The cumulative vertical displacement for one complete cycle of our model is shown in Figure 4. Despite several idealizations the principal effects of subduction are reproduced, since the footwall block of the fault is flexed downward and the plate has undergone an increment of subsidence into the asthenosphere. Aside from coseismic movements this effect is predominantly due to the viscoelastic reaction of the asthenosphere to surface faulting. This mechanism may appear to differ fundamentally from the conventional viewpoint that subduction is the result of an active downward drag exerted by

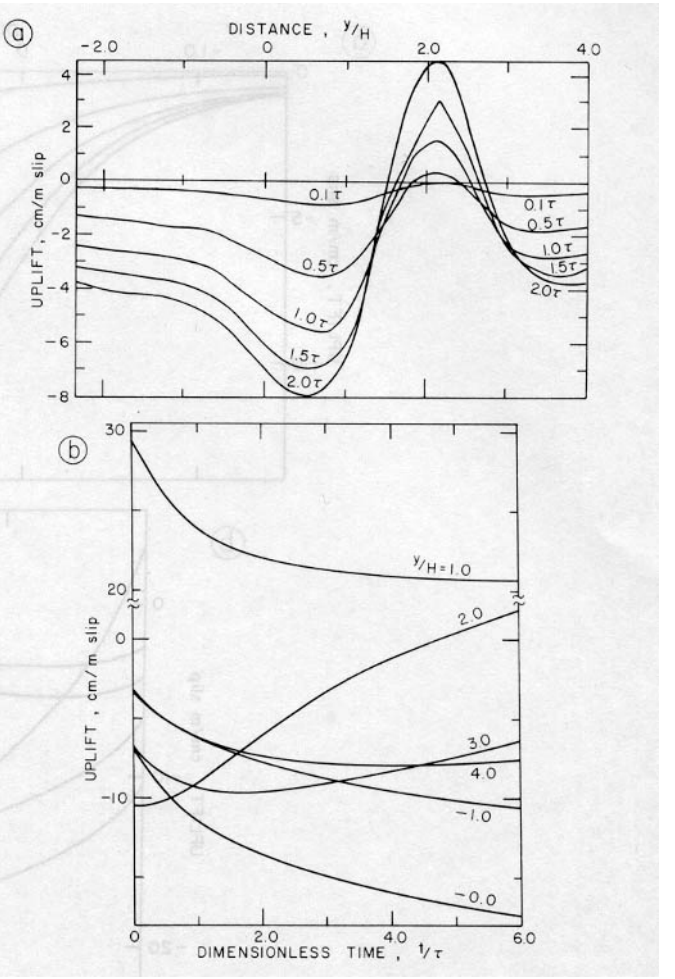

Fig. 3. (*a*, *b*) Similar to Figure 2 but for a fault dipping 30° and rupturing the entire thickness of the lithosphere. In Figure 3*b*, note the break in scale of the vertical coordinate axis between +2 and +20 cm.

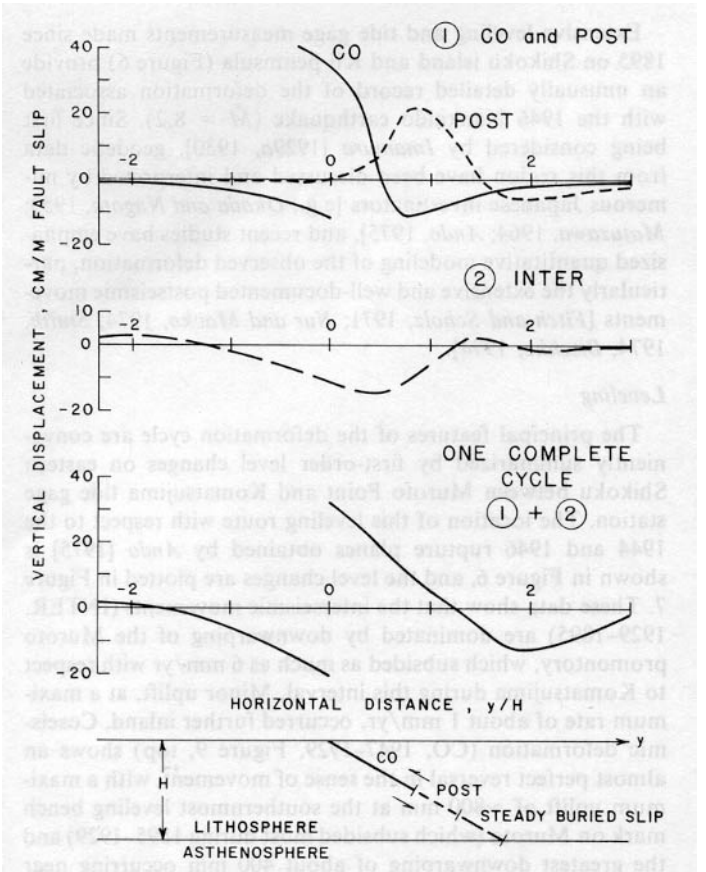

Fig. 4. Vertical displacement profiles for the model of the earthquake cycle proposed in this study. All curves are normalized for one meter of slip on the 30° inclined fault segment shown on the bottom of the figure, and perpendicular distance from the fault, y, is scaled by the lithospheric thickness H.

the cold, dense subducting plate. However, despite differences there is a basic underlying similarity. In both cases the plate-driving forces are the ultimate cause of the deformation, since in our model these forces (via the steady buried slip) load the shallow fault plane and produce the coseismic movements that lead to asthenospheric readjustments.

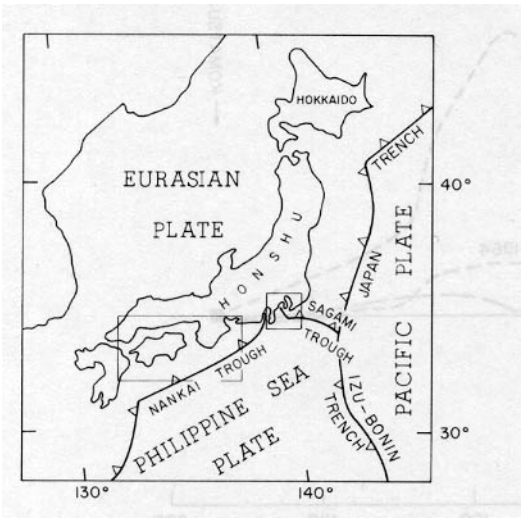

Fig. 5. Location map of Japan, showing major plates and subduction boundaries. Shaded boxes outline two regions where the vertical movement history through a major earthquake cycle is particularly well documented. Larger box shows the region of southwest Japan affected by the 1944 Tonankai and 1946 Nankaido earthquakes, and the smaller shaded area outlines the South Kanto region, site of a great earthquake in 1923.

Further Simplifying Assumptions

In comparing the modeling results of Figures 1, 2, 3, and 4 with observed deformation in underthrust zones, two details not included in our calculations deserve brief mention. First of all, our results consider the asthenospheric relaxation effects of only a single earthquake rather than the superposition of a periodic or irregular sequence of events. Thus our 'one-shot' model will always tend to underestimate somewhat the interseismic subsidence due to asthenospheric relaxation. The error incurred will depend on the ratio of recurrence interval T to asthenospheric relaxation time τ, and the approximation is best when T/τ is large and t/τ is small. In fitting data the net effect of this approximation will be to slightly underestimate the true asthenospheric viscosity, although for the modeling done here the error is not large.

Second, the long-term response of the asthenosphere to steady buried slip has not been modeled exactly, since our results are computed for slip occurring as a step function in time. Although the computations can easily be generalized to ramp time functions (Appendix B), the transient behavior in the asthenosphere persists long after slip is initiated, so obtaining the limiting steady state behavior is more difficult. However, whatever its details, the effect is significantly smaller than either the instantaneous elastic response of the buried slip or the asthenospheric relaxation to surface faulting. Furthermore, its uplift profile is quite similar to the purely elastic part of the deformation (see Figure 1*b*). For these reasons its effect does not play a critical role in model fitting, and we have accordingly included only the elastic response to steady buried slip in our modeling.

Although buoyant restoring forces are not included in our computations, an order of magnitude calculation suggests that for each cycle of strain accumulation and release, buoyancy effects are insignificant in comparison to viscous stresses induced by asthenospheric relaxation. Neglecting coseismic density perturbations, for a displacement ΔH of the lithosphere-asthenosphere boundary an upper bound to the incremental pressure on the lithosphere opposing this displacement is approximately $\rho g \Delta H$, where ρ is the density of the lithosphere and g is the acceleration due to gravity. If $\rho = 3.0$ g/cm^3, this pressure is about 0.3 bar/m of ΔH. Owing to recurrent great earthquakes the viscous stresses near the fault will never decay to values comparable to this, always remaining near the coseismic stress drop, a few tens of bars. However, these seismically imposed stresses decrease in amplitude away from the fault and become negligible beyond a few fault dimensions away from the trench, so neglect of buoyant stresses seems justified only within this range.

Note as well that we do not consider those buoyant effects that are due to the subduction of the downgoing lithospheric plate. These forces cannot be discussed independently of the other potential plate-driving and resisting forces, and our simplistic assumption has been that their net effect on the plate boundary deformation is to maintain steady buried slip beneath the shallow locked portion of the fault.

4. Observed Deformation in Southwest Japan

Active underthrusting of the Philippine Sea plate beneath southwestern Japan occurs along the Nankai Trough (Figure 5), and *Seno* [1977] has estimated the plate convergence rate here to be about 40 mm/yr, with the orientation of the slip

Fig. 6. Area of the 1944 Tonankai (M = 8.0) and 1946 Nankaido (M = 8.2) earthquakes in southwest Japan. Rectangles show surface projections of inferred coseismic fault planes as determined by *Ando* [1975]. The two westernmost rectangles are for the 1946 earthquake, and the eastern one outlines the inferred 1944 fault plane. Tide gage stations (triangles, with names) are referred to in the text, and parts of their sea level records are plotted in Figure 8. Dashed lines show leveling routes across eastern Shikoku and Kii Peninsula, for which elevation change data are plotted in Figures 7–9.

vector indicating that the relative motion occurring across this part of the plate boundary is predominantly reverse dip slip with a smaller component of right lateral strike slip movement. Subduction here is comparatively recent, and the absence of earthquakes deeper than about 100 km indicates that the underthrust plate has not yet penetrated below this depth [*Kanamori*, 1972].

Recurrent destructive earthquakes are a characteristic feature of the Nankai Trough in southwest Japan, and historical accounts document shocks as long ago as 684 A.D. and indicate repeat times of 100–200 years for major earthquakes in this region [*Imamura*, 1928; *Ando*, 1975]. Two great underthrust events occurred here in 1944 and 1946; the previous episode of rupturing on the Nankai Trough was in 1854.

Extensive leveling and tide gage measurements made since 1895 on Shikoku island and Kii peninsula (Figure 6) provide an unusually detailed record of the deformation associated with the 1946 Nankaido earthquake (M = 8.2). Since first being considered by *Imamura* [1929*a*, 1930], geodetic data from this region have been discussed and interpreted by numerous Japanese investigators [e.g., *Okada and Nagata*, 1953; *Matuzawa*, 1964; *Ando*, 1975], and recent studies have emphasized quantitative modeling of the observed deformation, particularly the extensive and well-documented postseismic movements [*Fitch and Scholz*, 1971; *Nur and Mavko*, 1974; *Smith*, 1974; *Bischke*, 1974].

Leveling

The principal features of the deformation cycle are conveniently summarized by first-order level changes on eastern Shikoku between Muroto Point and Komatsujima tide gage station. The location of this leveling route with respect to the 1944 and 1946 rupture planes obtained by *Ando* [1975] is shown in Figure 6, and the level changes are plotted in Figure 7. These data show that the interseismic movements (INTER, 1929–1895) are dominated by downwarping of the Muroto promontory, which subsided as much as 6 mm/yr with respect to Komatsujima during this interval. Minor uplift, at a maximum rate of about 1 mm/yr, occurred further inland. Coseismic deformation (CO, 1947–1929, Figure 9, top) shows an almost perfect reversal in the sense of movement, with a maximum uplift of ~800 mm at the southernmost leveling bench mark on Muroto (which subsided most during 1895–1929) and the greatest downwarping of about 400 mm occurring near where interseismic uplift was greatest. Level changes during 1947–1964 (POST 1) show that postseismic movements during this time involved predominantly land uplift, with maximum changes approaching 400 mm. The most recent leveling comparison available (1971–1964, POST 2) suggests a pattern of deformation somewhat intermediate between the POST 1 and INTER profiles.

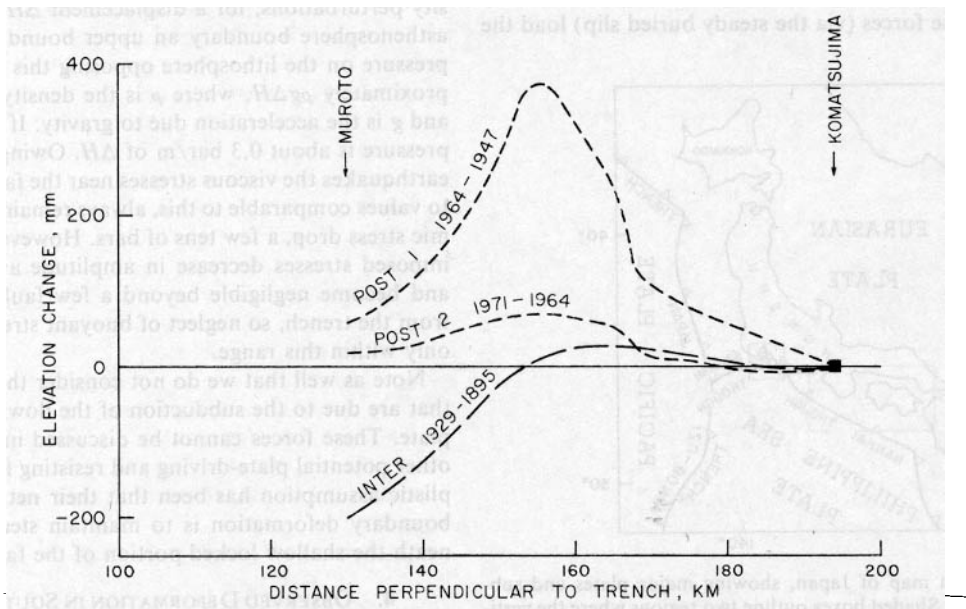

Fig. 7. Elevation changes in eastern Shikoku between Muroto Point and Komatsujima tide gage station. Komatsujima is assumed fixed in each time interval, and elevation changes are projected onto a profile perpendicular to the Nankai Trough. The 1929–1895 changes, typical of the interseismic secular deformation, are taken from *Imamura* [1930]. The 1964–1947 and 1971–1964 level changes, taken from unpublished data of the Geographical Survey Institute, show postseismic uplift due to the 1946 earthquake.

Leveling Datum

In Figures 7 and and 9 (top) we have followed *Imamura* [1930] and *Hayashi* [1970] in assuming that Komatsujima remained fixed during the interseismic and postseismic phases of the deformation. Although no continuous tide gage records were available during 1895–1929 to validate this assumption, leveling data from the Kii peninsula, ~60 km to the east of Komatsujima (see Figure 6), independently support Imamura's choice of datum level for eastern Shikoku. This leveling is tied to a continuously operating tide gage at Kushimoto (Figure 6), and with this absolute datum level as a tie, the 1929–1895 deformation profile from Kushimoto to Osaka given by *Imamura* [1929*a*] is very similar to that obtained further west on Shikoku by assuming that Komatsujima was fixed during 1895–1929. Although no record exists at Komatsujima during 1947–1950, continuous measurements made since 1951 show that the net change in sea level for 1951–1971 was 60 mm or less [*Coastal Movements Data Center*, 1976]. The coseismic profile shown in Figure 9 (top) is taken from a report of the *Geographical Survey Institute of Japan* [1954], in which it was assumed that bench marks on the Japan Sea coast of southwest Honshu remained unmoved during 1929–1947.

Short-Term Postseismic Movements

Data from sea level records and local-scale leveling in Shikoku provide further details on the short-term time dependence of the postseismic movements. Uplift time histories from four tide gages and one frequently repeated leveling segment are shown in Figure 8, and both the tidal stations and the level line are located in Figure 6. Although smoothed versions of these same tidal records have been reproduced many times [e.g., *Matuzawa*, 1964; *Nur and Mavko*, 1974], this smoothing gives a somewhat misleading impression of the precision of the observations, and Figure 8*a* shows the unsmoothed monthly means taken from *Kawasumi* [1956]. As the preearthquake sections show, noise levels on these records are

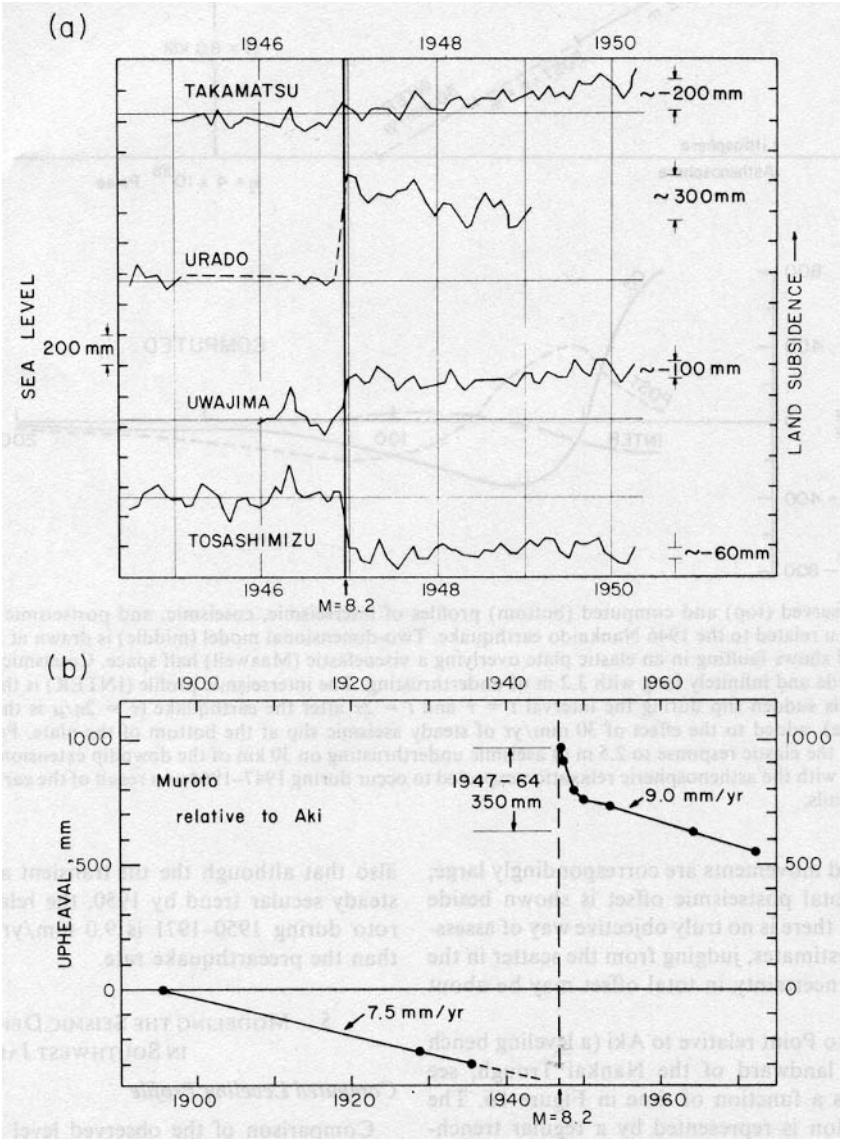

Fig. 8. Short-term postseismic changes related to 1946 Nankaido earthquake. (*a*) Monthly means of tide gage records for stations on Shikoku shown in Figure 6 [from *Kawasumi*, 1956]. Estimates of total postseismic offset are indicated for each record. Note that land subsidence is measured positive upward on these sea level records. (*b*) Elevation change of Muroto Point relative to Aki (locations in Figure 6) as determined from first-order leveling (data from *Okada and Nagata* [1953] and unpublished leveling, Geographical Survey Institute). Interseismic relative subsidence rate and corresponding rate during 1951–1971 are shown for reference, as is the total 1947–1964 elevation change between the two bench marks.

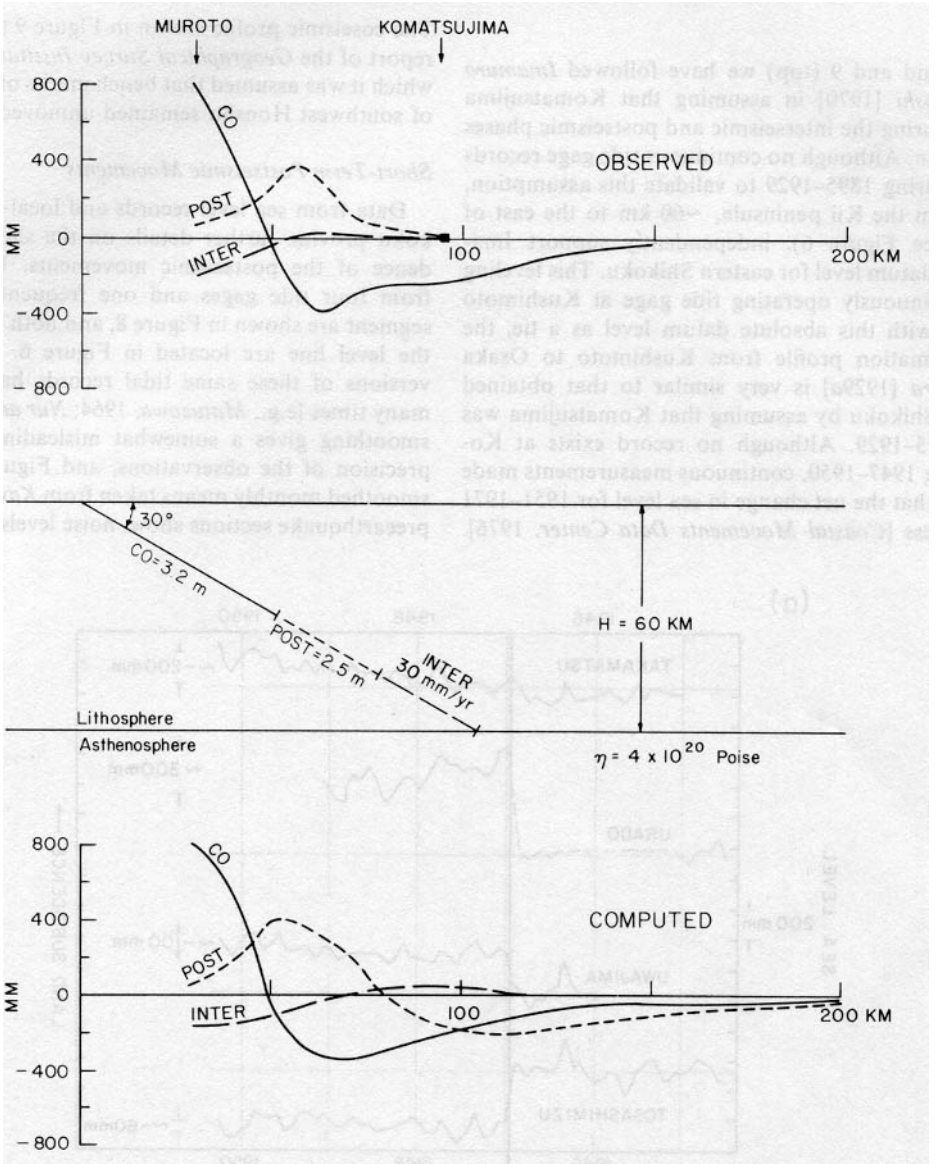

Fig. 9. Observed (top) and computed (bottom) profiles of interseismic, coseismic, and postseismic level changes in eastern Shikoku related to the 1946 Nankaido earthquake. Two-dimensional model (middle) is drawn at the same scale as the graphs and shows faulting in an elastic plate overlying a viscoelastic (Maxwell) half space. Coseismic model (CO) is a fault 60 km wide and infinitely long with 3.2 m of underthrusting. The interseismic profile (INTER) is the asthenospheric response to this sudden slip during the interval $t = \tau$ and $t = 2\tau$ after the earthquake ($\tau = 2\eta/\mu$ is the asthenospheric relaxation time), added to the effect of 30 mm/yr of steady aseismic slip at the bottom of the plate. Postseismic model (POST) shows the elastic response to 2.5 m of aseismic underthrusting on 30 km of the downdip extension of the coseismic rupture, along with the asthenospheric relaxation expected to occur during 1947–1964 as a result of the earthquake. See text for further details.

substantial, but ground movements are correspondingly large; our estimate of the total postseismic offset is shown beside each record. Although there is no truly objective way of assessing the error in these estimates, judging from the scatter in the 1944–1946 data, the uncertainty in total offset may be about ±50 mm.

The tilting of Muroto Point relative to Aki (a leveling bench mark 30 km further landward of the Nankai Trough, see Figure 6) is shown as a function of time in Figure 8*b*. The interseismic deformation is represented by a regular trenchward tilting of 7.5 mm/yr prior to 1946, and this trend is interrupted by the coseismic tilt offset of opposite sense, followed by a rapidly decaying transient. Note that the character of this transient agrees well with the postseismic uplift record of the Urado tide gage, located 40 km to the west of Aki. Note also that although the tilt transient appears to merge into a steady secular trend by 1950, the relative subsidence of Muroto during 1950–1971 is 9.0 mm/yr, still somewhat higher than the preearthquake rate.

5. Modeling the Seismic Deformation Cycle in Southwest Japan

Computed Leveling Profile

Comparison of the observed level changes in eastern Shikoku (Figure 7) with the model calculations of Figure 1 clearly makes the point we shall advocate here, that the postseismic uplift is predominantly the result of buried aseismic slip, while the observed interseismic downwarping is due principally to the effects of asthenospheric relaxation. Figure 9 compares the

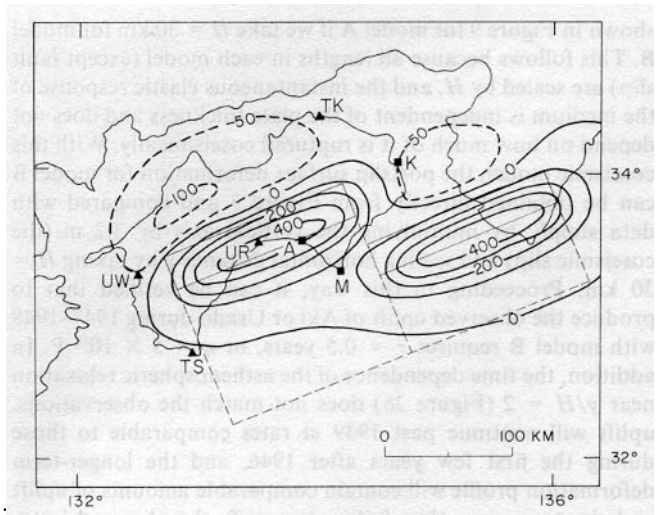

Fig. 10. Computed postseismic uplift in southwest Japan. Solid rectangles are surface projections of faults that are downdip extensions of *Ando*'s [1975] two coseismic fault planes (dashed rectangles). Tops of postseismic faults are at 30-km depth, faults are 30 km wide and 150 km long and dip 30° NNW, and each have 2 m of reverse dip slip and 1 m of right lateral strike slip movement across them. Contour interval is 100 mm except for addition of −50-mm contour. Solid triangles show tide gage stations of Figure 8*a* (UW is Uwajima, TS is Tosashimizu, UR is Urado, and TK is Takamatsu), and solid squares denote endpoints of leveling routes (A is Aki, M is Muroto, and K is Komatsujima).

Muroto-Komatsujima leveling observations with computations made using a simple two-dimensional model of faulting in an elastic lithosphere overlying a Maxwell asthenosphere. The plate thickness assumed is 60 km, close to *Kanamori*'s [1970] estimate of the lithospheric thickness for Japan obtained from the travel times of seismic body waves, and the asthenospheric viscosity is 4×10^{20} P (τ = 40 years). To fit the coseismic deformation in 1946, 3.2 m of slip occurs on a 30°-dipping fault that ruptures half the lithospheric thickness. Note that the Nankai Trough itself is located about 120 km off Muroto Point, while the surface trace of the coseismic fault in Figure 9 is only 30 km offshore. Such a landward shift of the coseismic fault plane is common to all models that fit the 1946 earthquake movements [*Fitch and Scholz*, 1971; *Ando*, 1975], and a similar effect is seen in models of other trench earthquakes [e.g., *Abe*, 1977]. This feature probably reflects a steepening and splaying of the main fault plane as it approaches the earth's surface, and this explanation also accounts for the discrepancy between the geodetically determined fault dip (~30°) and that obtained from the fault plane solution using seismic waves (dip ~10°; *Kanamori* [1972]).

TABLE Observed Versus Computed Postseismic Deformation for 1946 Nankaido Earthquake

Location	Time Interval	Observed Vertical Movement, mm	Computed (Aseismic Slip + Asthenosphere Relaxation), mm
Uwajima	1947–1950	−100	−70 (−50 − 20)
Tosashimizu	1947–1950	−60	−40 (−30 − 10)
Urado	1947–1948	+300	+400 (+420 − 20)
Takamatsu	1947–1950	−200	−50 (−40 − 10)
Aki-Muroto	1947–1964	+350	+350 (+360 − 10)
Maximum relative uplift, Muroto-Komatsujima leveling	1947–1964	+370	+220 (+250 − 30)

Postseismic uplift is modeled by imposing comparable amounts of aseismic slip (2.5 m of underthrusting) on 30 km of the downdip extension of the coseismic fault, and the computed profile also includes the effects of 17 years of asthenospheric relaxation following the earthquake. The interseismic deformation, actually primarily the result of the 1854 earthquakes (INTER profile is for 1895–1929), is due to asthenospheric relaxation between $t = \tau$ and $t = 2\tau$, supplemented by 30 mm/yr of steady aseismic slip on the bottom quarter of the lithosphere-wide megathrust, which in our model does not rupture in either the coseismic or postseismic phases of the deformation cycle. The rate of slip is close to *Seno*'s [1977] estimate of the dip slip component of the plate convergence rate.

Two considerations suggest that the estimate of asthenospheric viscosity obtained in our model is too low by a factor of 2–3. First, historic records of coastal deformation in 1854 [see *Ando*, 1975, Figure 8] suggest that in relation to the 1946 shock, coseismic slip was at least 50% greater in 1854. Since the asthenospheric relaxation scales linearly with the seismic slip, the same amount of downwarping between 1895 and 1929 can thus be obtained with a correspondingly higher asthenospheric viscosity. A second consistent bias results because the effects of earthquakes earlier than 1854 are not included in our model, and again these recurrent events would add to the deformation occurring in 1895–1929. For example, examination of Figure 2*b* indicates that the effects of the next previous Nankai Trough event in 1707 would still be substantial 200 years later, producing 4 cm of downwarping per meter of coseismic slip between $t = 5\tau$ and 6τ at $y/H = 1.0$. Approximately accounting for these biases in this way suggests that $\sim 10^{21}$ P may be a more appropriate value for the effective viscosity of the asthenosphere beneath southwest Japan.

Detailed Postseismic Model

In order to demonstrate that postseismic buried slip can also satisfactorily explain the shorter-term deformation exhibited by the tide gage and leveling data in Figure 8, we have computed the surface deformation due to a simple three-dimensional model whose geometry is suggested by *Ando*'s [1975] coseismic model (Figure 6) and our two-dimensional postseismic model (Figure 9). This three-dimensional model consists of two fault segments, each 150 km long and 30 km wide, that dip 30° WNW, that have their top edge at 30 km depth, and that each have 2 m of dip slip and 1 m of right lateral strike slip movement across them. The 2:1 ratio of reverse dip slip to strike slip motion is precisely that which *Ando* [1975] determined in his coseismic model, and as Figure 10 shows, the two aseismic fault planes are immediately adjacent to Ando's two coseismic faults.

Examination of Figure 10 and Table 1 demonstrates that this model, or obvious minor modifications to it, can explain all of the basic features of the observed postseismic deformation on Shikoku. The strikingly different behavior of Uwajima and Tosashimizu relative to Urado or Aki is seen to be due to the combination of an end effect of rupture termination and a minor asymmetry in the deformation contours that results from the small right lateral component to the motion. Table 1 shows that aided somewhat by the small amounts of subsidence expected from asthenospheric relaxation during 1947–1950, the computed vertical offsets at Uwajima and Tosashimizu provide a satisfactory match with the observations.

Although the uplift at Urado is overestimated by 100 mm, the observed value represents only deformation to early 1949, and the similarities between this tide gage recording and the Muroto-Aki tilt suggest the likelihood that an additional 100–150 mm of uplift occurred at Urado between 1949 and 1964. The observed downwarp of about 200 mm at Takamatsu is poorly accounted for by our model, and we can see no simple modification to it that will produce more than about 100 mm of subsidence so distant from the coseismic fault plane. The general shape of the computed deformation profile between Muroto and Komatsujima agrees well with observations. Although the maximum uplift is about 150 mm too small, a short eastward extension of the western fault segment will result in a better match. The model provides an excellent fit to the Muroto-Aki postseismic tilt offset to 1964. About 0.3 m of additional slip during 1964–1971 will adequately explain the continued tilting here as well as the level changes between Muroto and Komatsujima (POST 2, Figure 7), although judging from the growing similarities between post-1965 and pre-1946 deformation patterns seen in Figures 7 and 8*b*, the interseismic mechanisms of asthenospheric relaxation and steady buried slip are beginning to make significant contributions to the observed movements as well.

Finally, although the observed time-dependent features of the postseismic movements are not documented well enough to provide firm constraints for our model, these features can be readily accounted for by postulating appropriate time histories for the aseismic slip and its spatial growth. For example, the Urado record and the Muroto-Aki tilt history may be faithfully reflecting the slip-time function on the fault immediately beneath these locations, while the more uniform, smaller-amplitude movements seen on the other three sea level records might be attributed to the lateral and downdip growth of the aseismic slip zone on the fault, supplemented by the less impulsive effects of asthenospheric relaxation. Some evidence for downdip growth of slip comes from leveling carried out in 1950 and later in western Shikoku [see *Fitch and Scholz*, 1971, Figure 14; *Hayashi*, 1970, Figure I–10], which shows uplift of ~100 mm in northwestern Shikoku rather than the downwarping shown by our model, although our results are consistent with 1948–1950 level changes observed there.

An Alternative Model

Using results obtained in section 2, we can consider the applicability to the Nankaido data of a faulting model in which coseismic rupture breaks through the entire lithosphere. The surface displacements due to asthenospheric relaxation in one such model are shown in Figure 3, and a comparison of Figure 3*a* with the 1947–1964 postseismic profile in Figure 7 suggests that the observed post-1946 upwarping of southern Shikoku might be identified with the local postslip uplift shown near $y/H = 2.0$ in Figure 3*a*. This model is similar to one proposed by *Smith* [1974] and follows the spirit of *Nur and Mavko*'s [1974] suggestion that post-Nankaido earthquake movements are due predominantly to the effects of asthenospheric relaxation.

Although in some respects appealing, this model (call it model B) has several defects that we believe make it a less likely explanation of the Nankaido data than the model we have proposed (which we shall refer to as model A). The features of this alternative model and its consistency with observations can be seen by referring to the data profile in Figure 7 and the model calculations in Figure 3. First of all, model B will have the same computed coseismic profile as that shown in Figure 9 for model A if we take $H = 30$ km for model B. This follows because all lengths in each model (except fault slip) are scaled by H, and the instantaneous elastic response of the medium is independent of the plate thickness and does not depend on how much of it is ruptured coseismically. With this coseismic model, the postslip surface deformation for model B can be obtained directly from Figure 3 and compared with data simply by multiplying the vertical axis by 3.2 m (the coseismic slip) and scaling horizontal distance y by taking $H = 30$ km. Proceeding in this way, it can be verified that to produce the observed uplift of Aki or Urado during 1947–1948 with model B requires $\tau = 0.5$ years, or $\eta = 5 \times 10^{18}$ P. In addition, the time dependence of the asthenospheric relaxation near $y/H = 2$ (Figure 3*b*) does not match the observations: uplift will continue past 1949 at rates comparable to those during the first few years after 1946, and the longer-term deformation profile will contain comparable amounts of uplift and downwarping, thus failing to satisfy the observed interseismic movement pattern.

6. OBSERVED DEFORMATION IN THE SOUTH KANTO REGION

On its northern boundary the Philippine Sea plate is being subducted beneath the Eurasian plate along the Sagami Trough (Figure 5), and near the western edge of this boundary the $M = 8.1$, 1923 Kanto earthquake occurred. *Seno*'s [1977] analysis indicates ~30 mm/yr of relative plate motion here, with the preponderance of movement across the western end of the Sagami Trough being right lateral strike slip, supplemented by a smaller amount of reverse dip slip motion. Underthrusting is evidently quite recent in the South Kanto district, since no earthquakes deeper than about 80 km associated with the subduction of the Philippine Sea plate have been clearly identified here [*Tsumura*, 1973].

Great earthquakes apparently occur somewhat irregularly along the Sagami Trough, since historical accounts document a more extensive event in the same region in 1703 but no previous comparably large shock since 818 A.D. Uplifted marine terraces record at least four 1703-type earthquakes in the previous ~6000 years [*Matsuda et al.*, 1978].

Both seismic [*Kanamori*, 1971] and geodetic data [*Ando*, 1971, 1974] indicate that the 1923 earthquake involved shallow, oblique-angle underthrusting on a fault plane dipping 30° to 45°NE, with 6 m of right lateral strike slip movement and 3 m of reverse dip slip. The location map in Figure 11 shows the surface projection of the coseismic fault plane inferred by *Ando* [1971].

The leveling data used in this study have been taken from the Annual Report of First Order Leveling in Japan edited by the Geographical Survey Institute. Whenever possible, absolute datum levels have been established by ties between level lines and continuously recording tide gage stations [*Coastal Movements Data Center*, 1976]. The leveling profiles that we have constructed are generally similar to those used by *Scholz and Kato* [1978], who have made a recent study of the deformation history of the South Kanto region. Our postseismic and interseismic profiles differ somewhat from those shown by Scholz and Kato because for these time intervals we have used actual observed elevation changes rather than the smoothed interseismic and extrapolated postseismic level changes used by them.

Leveling

Figure 11 shows the locations of geodetic survey lines and tide gage stations we use here to summarize the characteristic

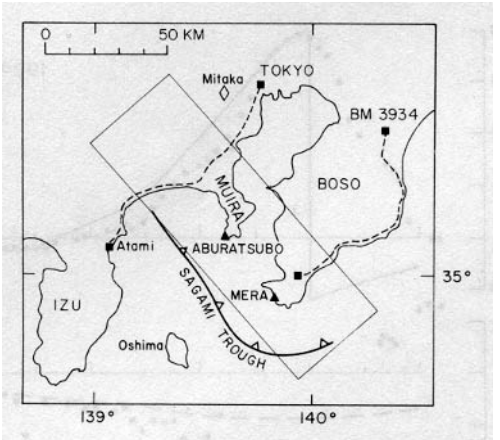

Fig. 11. South Kanto region, showing the coseismic fault plane of the 1923 earthquake determined by *Ando* [1971]. Leveling routes from Tokyo to Atami and on the eastern side of the Boso Peninsula are shown dashed, and data from these lines are plotted in Figures 12 and 13. Open diamond symbol shows the location of the chained rhombus at Mitaka, for which shear strain changes are plotted in Figure 14, and triangles locate Aburatsubo and Mera tide gage stations, whose sea level records are also shown in Figure 14.

features of the deformation cycle in the South Kanto region. The principal observations come from repeated first-order leveling surveys carried out since 1895 along two routes, from Tokyo to Atami, crossing the landward extension of the Sagami Trough, and along the east coast of the Boso peninsula, extending to within ~30 km of the subduction boundary.

Examination of the coseismic, postseismic, and interseismic

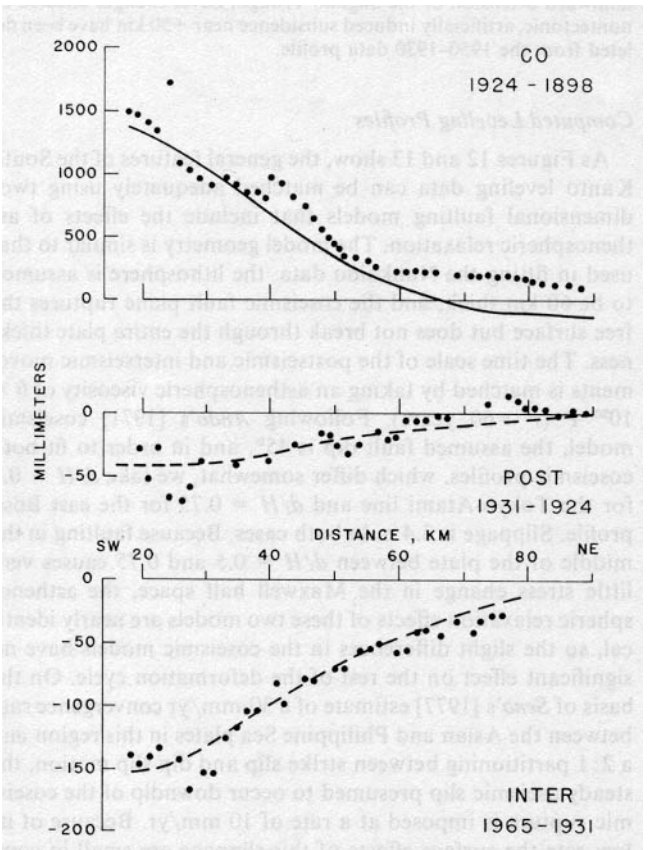

Fig. 12. Elevation changes from a leveling route on eastern side of the Boso peninsula. Data are projected onto a profile perpendicular to the Sagami Trough, which is the zero point for the profile. Solid and dashed lines show fit to the data of a model described in the text.

level changes on the east Boso route (Figure 12) illustrates clearly the two most distinctive features of the deformation cycle in the South Kanto region: first, that the postseismic vertical movements are very small and second, that they do not differ radically from the interseismic secular deformation. The subsidence rates do appear to be about a factor of 2 greater in the 7 years following 1923, but the spatial patterns of the POST and INTER movements are otherwise very similar. Although differences between the POST and INTER profiles do occur near the landward extension of the Sagami Trough on the Tokyo-Atami line (Figure 13), outside this narrow (~20 km wide) region the movement patterns seen on the two leveling routes are very similar and indicate predominantly downwarping in both the postseismic and interseismic time intervals. A comparison of Figure 12 with Figure 9 (top) shows clearly that the postseismic vertical movements in South Kanto differed very markedly from those that followed the 1946 Nankaido earthquake: on leveling segments in comparable positions with respect to the coseismic fault plane (refer to Figures 6 and 11), there were only modest amounts of downwarping in the 7 years after the Kanto earthquake (~−50 mm), while uplift of almost 400 mm occurred in the 17 years following the Nankaido earthquake.

Although the CO and INTER profiles for east Boso are generally similar to those for corresponding phases of the deformation cycle in southwest Japan, several significant differences are worth mentioning. First, distinct offsets clearly evident on the coseismic profile (near 25 and 40 km in Figure 12) are due to secondary faulting at the time of the 1923 earthquake [*Imamura*, 1929*b*; *Ando*, 1974; *Scholz and Kato*, 1978]. Second, the INTER profile does not steepen monotonically toward the Sagami Trough but instead flattens or perhaps even reverses its trend inside about 30-km distance from the trench. This feature is also seen, though rather less definitively, on the POST profile and also shows up well on the west Boso leveling data presented by *Scholz and Kato* [1978, Figure 8].

Additional differences and complexities in the deformation pattern within the South Kanto district are evident in the leveling results from the Tokyo-Atami line (Figure 13). Comparison with Figure 12 shows that the coseismic uplift is considerably narrower here, a feature that *Ando* [1971] has attributed to the asymmetry that results from the large right lateral component in the coseismic slip. Furthermore, the CO profile has no sharp offset near the Kozu-Matsuda fault, the landward extension of the Sagami Trough, but instead shows an irregular drop to zero level change between this fault trace and Atami. During the POST and INTER phases of the deformation cycle the Tokyo-Atami data exhibit considerable complexity within ~20 km of the Kozu-Matsuda fault, showing a sharp offset near −10 km in 1923–1930 and steep gradients centered near +10 km during 1930–1950. However, outside this region both the POST and INTER movements are very similar to those which occurred on the eastern side of Boso peninsula, about 70 km to the southeast.

Short-Term Postseismic Movements

In addition to the rather coarse time resolution provided by the leveling measurements, a smaller number of additional observations, summarized in Figure 14, provide more detail on the movements that occurred immediately after 1923 and show how, in a few locations at least, the postseismic movements gradually merged into the steady interseismic phase of the deformation cycle. Figure 14*a* shows shear strain changes de-

termined from repeated length measurements of a rhombus of about 100-m aperture located at Mitaka, near Tokyo (see Figure 11) and discussed previously by *Fujita* [1972] and *Scholz and Kato* [1978]. These results show that post-earthquake horizontal strain changes at Mitaka were remarkably large in comparison with post-1923 vertical deformation observed elsewhere in the South Kanto district, amounting by 1932 to more than one third of the coseismic strain drop. The data suggest that changes occurred episodically in two time intervals, during a 1-year period immediately following the earthquake, and spread over about 4 years in 1928–1932. The total change to 1935 is about 15 μstrain, and the plane of maximum right lateral shear straining has an azimuth of 138°, nearly parallel to the Sagami Trough and the strike of *Ando*'s [1971] coseismic fault. The time history of movements at Mitaka is somewhat reminiscent of the post-Nankaido tilt changes between Muroto and Aki (Figure 8*b*), although the time scale is somewhat longer at Mitaka. Note also that data from the nearby segments of the Tokyo-Atami leveling route, only about 10 km southeast of Mitaka, show that the large postseismic shear strain changes that occurred there were accompanied by only modest amounts of vertical deformation: 1923–1930 level changes are less than 40 mm, and corresponding tilts are about 1×10^{-6} rad, or about an order of magnitude smaller than the shear strain changes.

Tide gage recordings (Figure 14*b*) provide some constraints on the postseismic movements as well as giving precise estimates for the average rates of interseismic subsidence at the tips of Boso and Miura peninsulas. Sea level measurements made since 1896 at Aburatsubo indicate an average subsidence rate of 4 mm/yr since that time, and observations made since 1931 at Mera are also consistent with this average rate. Both tide gage records appear to show a slightly higher subsidence rate following the Kanto earthquake until about 1940, roughly 5–6 mm/yr, and a rather lower rate thereafter, about 3–4 mm/yr, although the indicated rate change is small and perilously close to the noise level of the observations.

7. Modeling the Seismic Deformation Cycle in the South Kanto Region

Although several features of the observed deformation in the South Kanto district are distinctively different from those occurring in southwest Japan, the same basic model is capable of explaining both sets of observations. The clearest differences are seen in the postseismic movements, and the almost universal subsidence shown in both the POST and INTER profiles for South Kanto, as well as their other general similarities, suggests that both are predominantly the result of asthenospheric relaxation. However, the Mitaka strain data provide a crucial clue that suggests that buried postseismic slip nontheless did occur after 1923, since the large and irregular movements observed at Mitaka cannot be adequately accounted for by asthenospheric relaxation, which can produce only modest, smoothly varing postseismic strain changes. The absence of comparable vertical deformation near Mitaka indicates that any buried slip that may be responsible for the movements occurring there must involve predominantly strike slip rather than dip slip fault motions. Such a predominance of strike slip over dip slip movements is also suggested by *Ando*'s [1971] coseismic model of the Kanto earthquake, and we shall show that with this same partitioning, modest amounts of postseismic slip (<1 m) can adequately satisfy the Mitaka strain data without violating the post-1923 leveling observations.

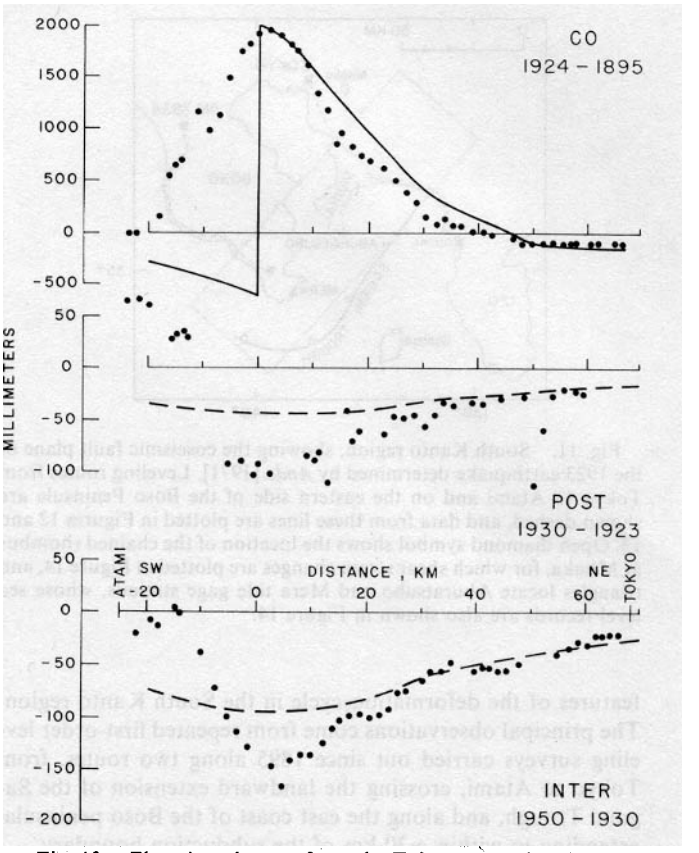

Fig. 13. Elevation changes from the Tokyo-Atami leveling route. Zero point on the profile is the Kozu-Matsuda fault, the presumed landward extension of the Sagami Trough. Level changes affected by nontectonic, artificially induced subsidence near +50 km have been deleted from the 1950–1930 data profile.

Computed Leveling Profiles

As Figures 12 and 13 show, the general features of the South Kanto leveling data can be matched adequately using two-dimensional faulting models that include the effects of asthenospheric relaxation. The model geometry is similar to that used in fitting the Nankaido data: the lithosphere is assumed to be 60 km thick, and the coseismic fault plane ruptures the free surface but does not break through the entire plate thickness. The time scale of the postseismic and interseismic movements is matched by taking an asthenospheric viscosity of 6×10^{20} P (τ =60 years). Following *Ando*'s [1971] coseismic model, the assumed fault dip is 45°, and in order to fit both coseismic profiles, which differ somewhat, we take d/H = 0.5 for the Tokyo-Atami line and d/H = 0.75 for the east Boso profile. Slippage is 3.4 m in both cases. Because faulting in the middle of the plate between d/H = 0.5 and 0.75 causes very little stress change in the Maxwell half space, the asthenospheric relaxation effects of these two models are nearly identical, so the slight differences in the coseismic models have no significant effect on the rest of the deformation cycle. On the basis of *Seno*'s [1977] estimate of a 30-mm/yr convergence rate between the Asian and Philippine Sea plates in this region and a 2:1 partitioning between strike slip and dip slip motion, the steady aseismic slip presumed to occur downdip of the coseismic rupture is imposed at a rate of 10 mm/yr. Because of its low rate the surface effects of this slippage are small in comparison with those due to asthenospheric relaxation. For the moment we assume that any effect of a dip slip component to the postseismic movements is small and can be safely ne-

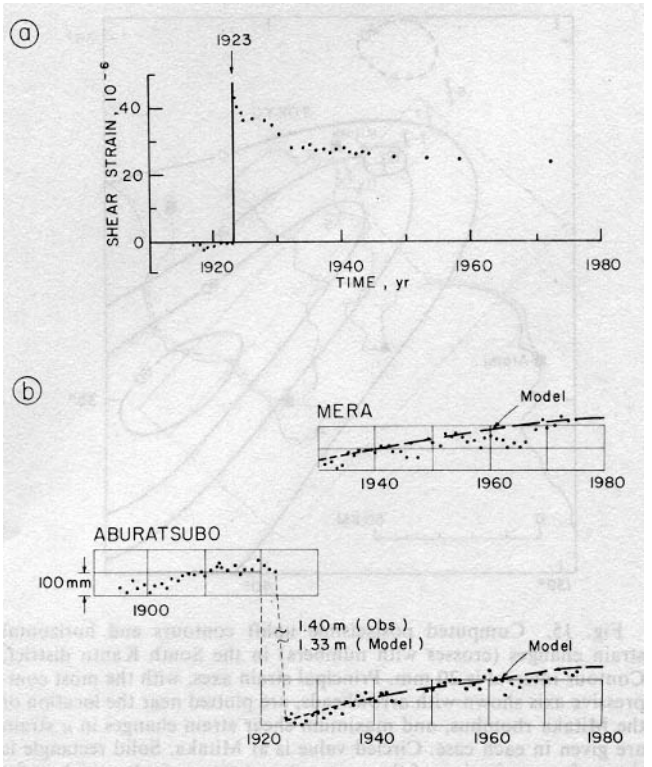

Fig. 14. Short-term postseismic changes related to the 1923 Kanto earthquake. (*a*) Shear strain changes versus time determined from chained length measurements of the Mitaka rhombus [from *Fujita*, 1972; *Scholz and Kato*, 1978]. Arbitrary zero level is taken in 1923 immediately before the earthquake. Shear strain is then calculated as the difference between the greatest and the least principal horizontal strains e_1 and e_3 referenced to this zero level. (*b*) Yearly mean sea level at Aburatsubo and Mera tide gage stations [*Coastal Movements Data Center*, 1976]. Dashed lines show the predicted deformation for a model of asthenospheric relaxation used to fit the leveling data of Figures 12 and 13 and described in the text.

glected, arguing this point later in our discussion of modeling the shear strain changes for the Mitaka rhombus.

For the east Boso level profile (Figure 12) both the shape and the amplitude of the computed POST and INTER curves match the observations quite well. Although *Scholz and Kato* [1978] have suggested that the shallowing in the trenchward tilt of the observed profiles inside ~30 km from the Sagami Trough is due to block tilting on the Boso peninsula, this feature can also be explained by our model as an effect of asthenospheric relaxation (recall Figure 1*a* and our earlier discussion of this feature of our model). The shape and level of the coseismic changes are successfully fitted, but details such as the secondary faulting offsets are not reproduced by the model.

The match of our model to the Tokyo-Atami data (Figure 13) is clearly not as good. Although satisfactory elsewhere, the CO model, which ruptures to the surface, completely fails to match the observations between −20 and 0 km on the profile. Although some improvement to the fit can be obtained by postulating that coseismic slip does not reach the surface [*Scholz and Kato*, 1978], the problem may lie elsewhere. We believe that the observed uplift in this region is due to a complex superposition of the effects of splay faulting and rupturing of semiconsolidated alluvial deposits, effects that are commonly observed in thrust faulting [e.g., *Buwalda and St. Amand*, 1955; *U.S. Geological Survey*, 1971] but which are difficult to reproduce quantitatively without using many near-surface fault segments [see *Jungels and Frazier*, 1973]. Although the mismatch between model and data is quite large, if our interpretation is correct, the effects on the Maxwell half space will be the same as those produced by surface rupturing, and accordingly we retain this model in calculating the deformation due to asthenospheric relaxation. With this model the general shape and amplitude of the POST profile from −10 to +60 km and the INTER profile more than 20 km from the Kozu-Matsuda fault are satisfied well. However, the computed profiles consistently underestimate the observed subsidence between +20 and −10 km. Furthermore, the sharp gradients near −10 km in the POST profile and around +10 km in the INTER phase of the deformation cannot be matched by a source as deep as the asthenosphere and must be due to deformation occurring at shallow depths. We do not attempt to model these complex fault zone movements, conceding that our preferred interpretation satisfies only the longer-wavelength features of deformation observed on the Tokyo-Atami leveling route.

Using our model derived from the leveling data, the time history of post-1923 vertical movements at the Mera and Aburatsubo tide gages in specified, and as Figure 14*b* shows, model calculations are in excellent agreement with observations. Not only is the general shape reproduced in each case, but the indicated decrease in subsidence rate is also matched by the slightly concave downward shape of the model curves: the average rate to 1940 is 5.4 mm/yr, and since 1940 the subsidence rate has been near 3.5 mm/yr. Because we have modeled the asthenospheric relaxation effects of only the 1923 event, our model cannot be used to fit the 1896–1923 tide gage record for Aburatsubo, since the movements during this time are due to the superimposed effects of previous great earthquakes in the Sagami Trough.

Detailed Postseismic Model

The asthenospheric relaxation models used to fit the postseismic leveling data cannot satisfy the large post- 1923 strain changes at Mitaka. However, two features of the observed movements suggest a modification to the POST models of Figures 12 and 13 that will leave the computed leveling profiles essentially unchanged yet will produce enough horizontal deformation to explain the Mitaka data. First of all, significant movements near Mitaka are largely horizontal, since nearby portions of the Tokyo-Atami leveling route show comparatively little contemporaneous tilting. Furthermore, the maximum right lateral shear at Mitaka is oriented nearly parallel to the Sagami Trough, so that the maximum compressive strain axis is not perpendicular to the trench but is rotated 45° counterclockwise with respect to it. Both observations suggest effects due predominantly to right lateral strike slip rather than reverse dip slip fault movements. The surface deformation effects produced by one satisfactory postseismic buried slip model that incorporates these features is shown in Figure 15. The slip ratio is 2:1 (0.6 m of strike slip, 0.3 m of reverse dip slip), and the fault plane, whose top edge is at 30-km depth, is 20 km wide and 130 km long and dips 45° NE. The dashed rectangle is the surface projection of Ando's coseismic fault plane, and the adjacent solid rectangle shows the corresponding postseismic fault.

Model results showing the orientation of the horizontal principal strains, their magnitudes, and the maximum right lateral shear (in microstrains) are plotted at Mitaka (circled) and nearby in Figure 15. Although the 1923–1935 observations are not matched exactly, minor modifications to the simple

model of Figure 15 can arbitrarily improve the fit. The computed value of γ_{12}, 10 μstrain, is less than that observed, but additional postslip shearing resulting from the asthensopheric relaxation due to the 6 m of right lateral coseismic slip (not modeled here) is probably sufficient to make up the difference. Alternatively, increasing only the strike slip component of the postseismic slip will accomplish the same purpose without measurably changing the vertical deformation field. The computed maximum compressive strain orientations agree with observations almost exactly (N6°E versus N3°E), but the observed ratio of maximum to minimum compressive strain is badly misfit (6.5 versus 0.3). However, as Figure 15 indicates, locations northwest of Mitaka show a favorable ratio, so this misfit can be remedied by shortening the postseismic fault by about 20 km at its northwestern end.

Relatively small amounts of postseismic uplift are produced by our buried slip model (Figure 15). The computed uplift pattern shows no sharp gradients across either the Tokyo-Atami or east Boso leveling routes, and maximum elevation changes along these lines are less than 40 mm. Long- wavelength level changes of this magnitude will not substantially alter the computed POST profiles (Figures 12 and 13) or the conclusions based on them, since any slight degradation in the model fit can be recovered by further modest changes in model parameters. Furthermore, the first postseismic survey on Boso peninsula was not carried out until nearly 1 year after the earthquake, and as Figure 14*a* shows, about half of the 1923–1935 shear straining occurred during this time. Note also that the east Boso POST profile cannot be tied to an absolute datum, and we have merely assumed that BM 3934 (Figure 11) remained fixed during 1924–1931. If this inference is in error, there is an additional degree of freedom available in modeling the POST data on Boso peninsula.

Finally, the postseismic straining at Mitaka is not easily explained by the back slip model proposed by *Fitch and Scholz* [1971] and *Scholz and Kato* [1978] to account for post-earthquake vertical deformation in southwestern Japan and in the South Kanto district. In this model, postseismic slip is postulated to act in opposite sense to the coseismic clip, implying left lateral normal faulting after the Kanto earthquake. Clearly, such movements on the coseismic fault or its downward extension will not result in a satisfactory fit to the 1923–1935 Mitaka data, which require the maximum right lateral shear strain direction to be parallel to the strike of the coseismic fault plane.

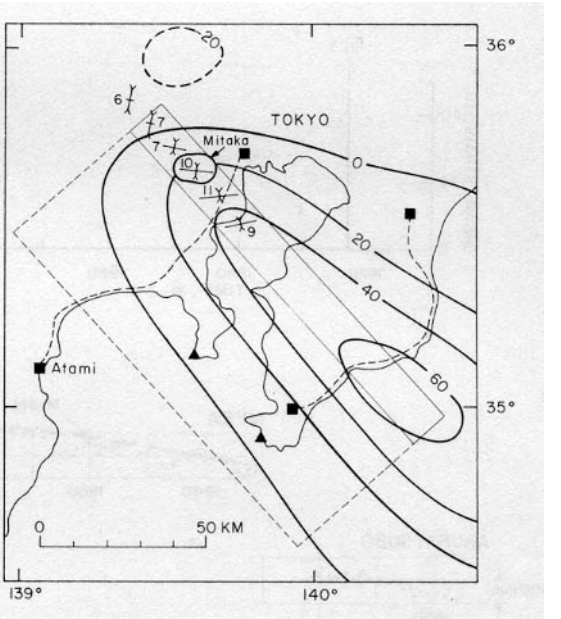

Fig. 15. Computed postseismic uplift contours and horizontal strain changes (crosses with numbers) in the South Kanto district. Contour interval is 20 mm. Principal strain axes, with the most compressive axis shown with arrowheads, are plotted near the location of the Mitaka rhombus, and maximum shear strain changes in μ strain are given in each case. Circled value is at Mitaka. Solid rectangle is the surface projection of the assumed postseismic fault, which is the downdip extension of *Ando*'s [1971] coseismic fault plane (dashed rectangle). Top of postseismic fault is at 30-km depth, and this fault is 20 km wide and 130 km long, dips 45° NE, and has 0.6 m of right lateral strike slip and 0.3 m of reverse dip slip movement across it. Solid squares and dashed lines show leveling routes, and solid triangles locate Aburatsubo and Mera tide gage stations.

8. Summary and Discussion

Our calculations have indicated that with conventional values of lithospheric thickenss and asthenospheric viscosity the interseismic subsidence observed landward of the major subduction zones off Japan can be understood as predominantly an effect of asthenospheric relaxation following major trench earthquakes, supplemented by steady aseismic slip on the deeper parts of the plate boundary, while the sometimes spectacular deformation episodes that follow great underthrust earthquakes in Japan and elsewhere are adequately explained by buried aseismic slip that acts in the same sense as the coseismic movements and occurs on the downdip extension of the coseismic fault plane. Although the effects of asthenospheric relaxation on observed postseismic movements are in general much smaller, data from the South Kanto region suggest that they can nonetheless be locally significant.

The model used here is obviously quite idealized in several respects. The effects of plate motion on subduction boundary deformation are approximated kinematically by imposing steady slip at the relative motion rate on the bottom segment of the plate bounding fault, thus evading explicit consideration of the forces that drive the plates. Any surface deformation effects that may be due directly to the downward pull of the subducting oceanic lithosphere are ignored in our model. If this process is important, its effects may be very similar to asthenospheric relaxation and produce downwarping of the overlying continental lithospheric plate. However, one line of evidence suggests that although this mechanism may make some contribution to the observed deformation, its effect is not a dominant factor. Finite element simulations of the gravitational pull of the underthrust slab made by *Bischke* [1974] indicate that although surface downwarping does occur, strains in the overlying continental plate are dominantly tensional. Thus some other mechanism is needed to match the interseismic horizontal deformation measured landward of trenches, which shows compressive straining oriented roughly parallel to the relative plate motion direction [see *Mogi*, 1970]. Though other models may also be able to generate the required compression, this feature is readily accounted for in our interseismic model, since both buried slip and asthenospheric relaxation produce largely compressional strains at the surface on the hanging wall block of the fault.

A further shortcoming of our model is its neglect in considering any modifications to asthenospheric flow that may result from the presence of a long subducted slab in the upper mantle beneath the continental plate. However, since the underthrust Philippine Sea plate has not yet penetrated below 100 km beneath either southwestern Japan or the South Kanto region,

neglect of both subduction effects may be justified for the model calculations made here. Furthermore, in both northern Honshu and Hokkaido (see Figure 5) the subducted Pacific plate is nearly 2000 km long and reaches depths in excess of 700 km, yet the pattern of interseismic subsidence [see *Kato*, 1979; *Seno*, 1979; *Shimazaki*, 1974] closely matches that occurring landward of the Nankai and Sagami troughs. This comparison suggests that the length of underthrust slab has little effect on the surface deformation and may indicate that similar processes are responsible for the interseismic deformation observed in both regions.

Although the deformation model proposed here is certainly not unique, our analysis does indicate that in underthrust zones the deformation effects of asthenospheric relaxation are likely to be quite significant and cannot be safely ignored. While our model may not match all features of the observations significantly better than other models [*Fitch and Scholz*, 1971; *Nur and Mavko*, 1974; *Smith*, 1974; *Bischke*, 1974; *Scholz and Kato*, 1978], it not only provides an adequate fit to the entire deformation cycle but does so without requiring extreme or exotic properties for the lithosphere and asthenosphere or ad hoc slip laws for the plate boundary megathrust. While our choice of lithospheric thickness, 60 km, is consistent with seismic estimates and the value determined for asthenospheric viscosity, 10^{21} P, agrees with independent determinations from studies of isostatic rebound, our conclusions are not strongly tied to these choices, and changes by as much as factors of 2–3 in these model parameters would not substantially alter our interpretation. Furthermore, if standard estimates of lithospheric thickness, asthenospheric viscosity, and depth of coseismic underthrusting are even approximately correct, something like the asthenospheric relaxation effects we have modeled here must occur at subduction zones. In addition, the predicted effects of asthenospheric relaxation produce deformation that agrees with observations and cannot be simply matched by dislocation models. These characteristics contrast significantly with the analogous situation at strike slip plate boundaries, where features of the observed deformation can be accounted for with half space dislocation models and where the shallow depth of coseismic faulting makes it somewhat less likely that asthenospheric relaxation contributes significantly to the surface movement pattern.

APPENDIX A

Rundle [1978] has shown how to compute the surface uplifts due to a finite, rectangular thrust fault. Here we specialize to the case of an infinitely long fault. From *Rundle* [1978, equation (2)] the uplift can be written as

$$u_z = \int_S ds \int_0^\infty \left\{ \left[X_{10}(0) J_0(kr) + X_{12}(0) J_2(kr) \cos 2\varphi \right] \sin 2\theta + X_{11}(0) J_1(kr) \sin \varphi \cos 2\theta \right\} k\, dk \qquad \text{(A1)}$$

where all quantities are as defined in *Rundle* [1978]. The integral over x' reduces to an integral from $(y - y')$ to infinity. Since the kernel functions $X_{1m}(0)$ contain only the source depth h, layer thickness H, and Fourier wave number k, the x' integral can be performed analytically [*Erdelyi et al.*, 1954]:

$$u_z = 2\int_0^\infty dk \int_{\xi_1}^{\xi_2} \left\{ \left[X_{10}(0) + X_{12}(0) \right] \cos k(y - y') \sin 2\theta + X_{11}(0) \sin k(y - y') \cos 2\theta \right\} d\xi \qquad \text{(A2)}$$

where $y' = h \cot\theta = \xi \cos\theta$ is the horizontal source coordinate as given by *Rundle* [1978]. Note that the kernels $X_{10}(0)$, $X_{11}(0)$, and $X_{12}(0)$ can be viewed as distributions on k for fixed values of h (and thus y' or ξ). If we can define an 'average' $\bar{k}$ such that

$$u_z \cong 2\int_{\xi_1}^{\xi_2} \left\{ \left[\bar{X}_{10}(0) + \bar{X}_{12}(0) \right] \cos \bar{k}(y - y') \sin 2\theta + \bar{X}_{11}(0) \sin \bar{k}(y - y') \cos 2\theta \right\} d\xi \qquad \text{(A3)}$$

then we expect the solution for the infinitely long fault to be periodic in y. That this in fact is the case can be verified by actual calculation. Many such infinite problems in mathematical physics display similar 'unphyiscal' characteristics and reflect the general conclusion that the solution is only valid near the source. For example, beyond the area shown in Figure 1*a* there are regions of significant uplift and downwarping that exhibit approximate periodic behavior. Furthermore, because of the assumed two-dimensional nature of the fault model, the displacements remain finite as $y \to \infty$. It can be readily shown, however, that for three-dimensional models, displacements tend to zero as the radial polar coordinate $r \to \infty$.

Finally, for both two- and three-dimensional fault models it can be demonstrated that the net volume change during the viscoelastic relaxation is zero, as it should be for an isothermal process. This is most easily seen by considering the viscoelastic solutions in the Laplace transform domain. There, the viscoelastic solutions are merely the static elastic solutions with the bulk and shear moduli replaced by functions of the transform variable s. Thus the transformed viscoelastic solutions have precisely the same spatial dependence as the corresponding static elastic solutions. The Laplace transform operation is linear in s, and so the final time-dependent viscoelastic solutions are just linear superpositions of the s-dependent transform domain solutions. Each elastic solution is a constant volume one, so a linear combination of them must be so as well.

APPENDIX B

Rundle [1978] gave the functions $\xi_n(t)$ for the case where the loading on the fault was a Heaviside step $H(t)$ in time. For the case of a Heaviside ramp $R(t)$ a reasonable approximation to steady slip, it can easily be verified that the result is

$$\xi_n(t) = V\left\{ R(t) - \tau H(t)\left[n - e^{-t/\tau} \sum_{m=0}^{n-1} \sum_{p=0}^{m} \frac{1}{p!}\left(\frac{t}{\tau}\right)^p \right] \right\} \qquad \text{(B1)}$$

where τ is the relaxation time defined by *Rundle* [1978] and V is the constant relative slip velocity. For the Maxwell rheology used in this paper, $\tau = 2\eta/\mu$, where η is the effective viscosity and μ is the rigidity. A superposition of ramp loads at different times can be used to represent a fault sliding steadily for some finite time. The corresponding functions $\xi_n(t)$ are then similar superpositions of (B1).

Acknowledgments. Discussion with D. J. Andrews, T. J. Fitch, T. C. Hanks, K. Kasahara, A. H. Lachenbruch, M. K. McNutt, J. C. Savage, C. H. Scholz, and A. T. Smith resulted in considerable improvement in the manuscript. M. Ando provided helpful comments on Japanese tide gage measurements and supplied an elusive reprint. This work was supported in part by a contract from the U.S. Department of Energy to Sandia Laboratories.

REFERENCES

Abe, K., Tectonic implications of the large Shioya-oki earthquakes of 1938, *Tectonophysics, 41*, 269–289, 1977.

Anderson, D. L., Accelerated plate tectonics, *Science, 187,* 1077–1079, 1975.

Ando, M., A fault-origin model of the great Kanto earthquake of 1923 as deduced from geodetic data, *Bull. Earthquake Res. Inst. Tokyo Univ., 49,* 19–32, 1971.

Ando, M., Seismotectonics of the 1923 Kanto earthquake, *J. Phys. Earth, 22,* 263–277, 1974.

Ando, M., Source mechanisms and tectonic significance of historical earthquakes along the Nankai trough, Japan, *Tectonophysics, 27,* 119–140, 1975.

Bischke, R. E., A model of convergent plate margins based on the recent tectonics of Shikoku, Japan, *J. Geophys. Res., 79,* 4845–4857, 1974.

Bott, M. H. P., and D. S. Dean, Stress diffusion from plate boundaries, *Nature, 243,* 339–341, 1973.

Brown, L. D., R. E. Reilinger, S. D. Holdahl, and E. I. Balazs, Postseismic crustal uplift near Anchorage, Alaska, *J. Geophys. Res., 82,* 3369–3378, 1977.

Buwalda, J. P., and P. St. Amand, Geological effects of the Arvin-Tehachapi earthquake, Earthquakes in Kern County, California, During 1952, *Bull. 171,* pp. 41–56, State of Calif. Dep. of Natur. Res., Div. of Mines, Sacramento, 1955.

Chinnery, M. A., Deformation of the ground around surface faults, *Bull. Seismol. Soc. Amer., 51,* 355–372, 1961.

Coastal Movements Data Center, *Table and Graphs of Annual Mean Sea Level Along the Japanese Coast,* 37 pp., Tokyo, 1976.

Elsasser, W. M., Convection and stress propagation in the upper mantle, in *The Application of Modern Physics to the Earth and Planetary Interiors,* edited by S. K. Runcorn, pp. 223–246, Interscience, New York, 1969.

Erdelyi, A., W. Magnus, F. Oberhettinger, and F. G. Tricomi, *Tables of Integral Transforms,* vol. II, McGraw-Hill, New York, 1954.

Fitch, T. J., and C. H. Scholz, Mechanism of underthrusting in southwest Japan: A model of convergent plate interactions, *J. Geophys. Res., 76,* 7260–7292, 1971.

Fujita, N., Deformation of the rhombus base line at Mitaka (in Japanese), *J. Geod. Soc. Jap., 18,* 8–16, 1972.

Fung, Y. C., *Foundations of Solid Mechanics,* Prentice-Hall, Englewood Cliffs, N. J., 1965.

Geographical Survey Institute of Japan, Resurvey of the south-western part of Japan after the great Nankaido earthquake of 1946, *J. Geogr. Surv. Inst. Jap., 4,* 1–69, 1954.

Hastie, L. M., and J. C. Savage, A dislocation model for the 1964 Alaska earthquake, *Bull. Seismol. Soc. Amer., 60,* 1389–1392, 1970.

Hayashi, T., A study of vertical movements of the earth's crust by means of the precise leveling, *Bull. Geogr. Surv. Inst., 15,* 1–69, 1970.

Imamura, A., On the seismic activity of central Japan, *Jap. J. Astron. Geophys., 6,* 119–137, 1928.

Imamura, A., On the chronic and acute earth-tilting in the Kii Peninsula, *Jap. J. Astron. Geophys., 7,* 31–45, 1929*a*.

Imamura, A., On the multiple source of origin of the great Kanto earthquake and its relation to the fault system connected with the earthquake, *Proc. Jap. Acad., 5,* 330–333, 1929*b*.

Imamura, A., On the chronic and acute earth-tilting in the southern part of Shikoku, *Jap. J. Astron. Geophys., 8,* 29–37, 1930.

Jungels, P. H., and G. A. Frazier, Finite element analysis of the residual displacements for an earthquake rupture: Source parameters of the San Fernando earthquake, *J. Geophys. Res., 78,* 5062–5083, 1973.

Kanamori, H., Mantle beneath the Japanese arc, *Phys. Earth Planet. Interiors, 3,* 475–483, 1970.

Kanamori, H., Faulting of the great Kanto earthquake as revealed by seismological data, *Bull. Earthquake Res. Inst. Tokyo Univ., 49,* 13–18, 1971.

Kanamori, H., Tectonic implications of the 1944 Tonankai and the 1946 Nankaido earthquakes, *Phys. Earth Planet. Interiors, 5,* 129–139, 1972.

Kasahara, K., Aseismic faulting following the 1973 Nemuro-oki earthquake, Hokkaido, Japan (a possibility), *Pure Appl. Geophys., 113,* 127–139, 1975.

Kato, T., Recent crustal movement in the Tohoku district for the period 1900–1975, *Tectonophysics,* in press, 1979.

Kawasumi, H., Crustal deformation in the Shikoku district as deduced from tide gage records, Second report (in Japanese), *Shikoku-Chiho Sogo Kaihatsu Shingikai,* 30–36, 1956.

Matsuda, T., Y. Ota, M. Ando, and N. Yonekura, Fault mechanism and recurrence time of major earthquakes in southern Kanto district, Japan as deduced from coastal terrace data, *Geol. Soc. Amer. Bull., 89,* 1610–1618, 1978.

Matuzawa, T., *Study of Earthquakes,* 213 pp., Uno Shoten, Tokyo, 1964.

Melosh, H. J., Nonlinear stress propagation in the earth's upper mantle, *J. Geophys. Res., 81,* 5621–5632, 1976.

Melosh, H. J., Reply, *J. Geophys. Res., 83,* 5009–5010, 1978.

Mogi, K., Recent horizontal deformation of the earth's crust and tectonic activity in Japan, 1, *Bull. Earthquake Res. Inst. Tokyo Univ., 48,* 413–430, 1970.

Nur, A., and G. Mavko, Postseismic viscoelastic rebound, *Science, 183,* 204–206, 1974.

Okada, A., and T. Nagata, Land deformation of the neighborhood of Muroto Point after the Nankaido great earthquake in 1946, *Bull. Earthquake Res. Inst. Tokyo Univ., 31,* 169–177, 1953.

Peltier, W. R., Glacial-isostatic adjustment, II, The inverse problem, *Geophys. J. Roy. Astron. Soc., 46,* 669–705, 1976.

Rundle, J. B., Viscoelastic crustal deformation by finite, quasi-static sources, *J. Geophys. Res., 83,* 5937–5945, 1978.

Rundle, J. B., and D. D. Jackson, A kinematic viscoelastic model of the San Francisco earthquake of 1906, *Geophys. J. Roy. Astron. Soc., 50,* 441–458, 1977.

Savage, J. C., and R. O. Burford, Accumulation of tectonic strain in California, *Bull. Seismol. Soc. Amer., 60,* 1877–1896, 1970.

Savage, J. C., and R. O. Burford, Geodetic determination of relative plate motion in central California, *J. Geophys. Res., 78,* 832–845, 1973.

Savage, J. C., and W. H. Prescott, Comments on 'Nonlinear stress propagation in the earth's upper mantle' by H. J. Melosh, *J. Geophys. Res., 83,* 5005–5007, 1978*a*.

Savage, J. C., and W. H. Prescott, Asthenosphere readjustment and the earthquake cycle, *J. Geophys. Res., 83,* 3369–3376, 1978*b*.

Scholz, C. H., and T. Kato, The behaviour of a convergent plate boundary: Crustal deformation in the South Kanto district, Japan, *J. Geophys. Res., 83,* 783–797, 1978.

Seno, T., Instantaneous rotation vector of Philippine Sea plate relative to the Eurasian plate, *Tectonophysics, 42,* 209–226, 1977.

Seno, T., Intraplate seismicity in Tohoku and Hokkaido and large interplate earthquakes: A possibility of a large interplate earthquake off the southern Sanriku coast, northern Japan, *J. Phys. Earth,* in press, 1979.

Shimazaki, K., Pre-seismic crustal deformation caused by an underthrusting oceanic plate, in eastern Hokkaido, Japan, *Phys. Earth Planet. Interiors, 8,* 148–157, 1974.

Smith, A. T., Time-dependent strain accumulation and release at island arcs: Implications for the 1946 Nankaido earthquake, Ph.D. thesis, 295 pp., Mass. Inst. of Technol., Cambridge, 1974.

Spence, D. A., and D. L. Turcotte, Viscoelastic damping of cyclic displacements on the San Andreas fault, *Proc. Roy. Soc., Ser. A,* in press, 1979.

Thatcher, W., Strain release mechanism of the 1906 San Francisco earthquake, *Science, 184,* 1283–1285, 1974.

Thatcher, W., Strain accumulation and release mechanism of the 1906 San Francisco earthquake, *J. Geophys. Res., 80,* 4862–4872, 1975.

Tsumura, K., Microearthquake activity in the Kanto district (in Japanese), *Publication for the 50th Anniversary of the Great Kanto Earthquake,* pp. 67–87, Earthquake Research Institute, Tokyo University, Tokyo, 1973.

U.S. Geological Survey, Surface faulting, The San Fernando, California, Earthquake of February 9, 1971, *U.S. Geol. Surv. Prof. Pap., 733,* 55–76, 1971.

Walcott, R. I., Structure of the earth from glacio-isostatic rebound, *Annu. Rev. Earth. Planet. Sci., 1,* 15–37, 1973.

(Received September 5, 1978;
revised April 23, 1979;
accepted April 23, 1979.)